JASN

GATM, renal Fanconi syndrome and kidney failure

Complete List of Authors:	Reichold, Markus; University of Regensburg, Medical Cell Biology Klootwijk, Riko; Medical Genetics Branch, NHGRI, NIH; 4 Department of Medicine, University College Reinders, Joerg; University of Regensburg, Institute of Functional Genomics Otto, Edgar; University of Michigan, Department of Pediatrics Milani, Mario; CNR-Biophysics Institute Broeker, Carsten; University of Regensburg, Medical Cell Biology Laing, Chris; University College London, Centre for Nephrology Wiesner, Julia; University of Regensburg, Medical Cell Biology Devi, Sulochana; University of Michigan Department of Pediatrics and Communicable Diseases Zhou, Weibin; University of Michigan, Department of Pediatrics Schmitt, Roland; University of Regensburg, Medical Cell Biology Tegtmeier, Ines; University of Regensburg, Medical Cell Biology Sterner, Christina; University of Regensburg, Medical Cell Biology Doellerer, Hannes; University of Regensburg, Medical Cell Biology Renner, Kathrin; University of Regensburg, Department of Internal Medicine III Oefner, Peter; University of Regensburg, Institute of Functional Genomics Dettmer, Katja; University of Regensburg, Institute of functional genomics Simbuerger, Johann; University of Regensburg, Institute of Functional Genomics Witzgall, Ralph; University of Regensburg, Institute for Molecular and Cellular Anatomy Stanescu, Horia; University College London, Centre for Nephrology Dumitriu, Simona; University College London, Centre for Nephrology Iancu, Daniela; University College London, Centre for Nephrology Patel, Vaksha; University College London, Centre for Nephrology Mozere, Monika; University College London, Centre for Nephrology Tekman, Mehmet; University College London, Centre for Nephrology Jaureguiberry, Graciana; University College London, Centre for Nephrology Issler, Naomi; Centre for Nephrology & ICH, University College London, Kesselheim, Anne; University College London, Centre for Nephrology Walsh, Stephen; CNRS-Université de Nice, Laboratoire de Physiologie des Membranes Cellulaires; University College London, Centre for Nephrology and Department of Physiology Gale, Daniel; University College London, Centre for Nephrology Howie, Alexander; University College London, Centre for Nephrology

Martins, Joana; University of Zurich, Institute of Anatomy
Hall, Andrew; University of Zurich, Institute of Anatomy
Kashgarian, Michael; Yale University School of Mdicine, Pathology
O'Brien, Kevin; NIH, NHGRI
Ferreira, Carlos; NIH, NHGRI
Atwal, Paldeep; Mayo Clinic
Jain, Mahim; Kennedy Krieger Institute
Hammers, Alexander; King's College London
Charles-Edwards, Geoffrey; Guy's & St Thomas' NHS Foundation Trust, Medical Physics
Choe, Chi-Un; University of Hamburg, Department of Neurology
Isbrandt, Dirk; University of Cologne, DZNE RG Experimental Neurophysiology
Cebrian-Serrano, Alberto; University of Oxford, Wellcome Trust Centre for Human Genetics
Davies, Ben; University of Oxford, Wellcome Trust Centre for Human Genetics
Sandford, Richard; Cambridge Univ., Medical Genetics
Pugh, Christopher; University of Oxford, Centre for Cellular and Molecular Physiology
Konecki, David; GeneDX
Povey, Sue; Univeristy College, London, Genetics, Evolution and the Environment
Bockenhauer, Detlef; Great Ormond Street Hospital for Children NHS Trust, ; University College London Medical School, Centre for Nephrology
Lichter-Konecki, Uta; University of Pittsburgh, Division of Medical Genetics
Gahl, William
Unwin, Robert; University College London, Centre for Nephrology
Warth, Richard; University of Regensburg, Medical Cell Biology;
Kleta, Robert; University College London,

Keywords:	AGAT, mitochondriopathy, tubulopathy, protein deposits, fibrosis

1
2
3
4
5
6
7
8
9
10
11
12
13
14
15
16
17
18
19
20
21
22
23
24
25
26
27
28
29
30
31
32
33
34
35
36
37
38
39
40
41
42
43
44
45
46
47
48
49
50
51
52
53
54
55
56
57
58
59
60

GATM, renal Fanconi syndrome and kidney failure

Markus Reichold[1#], Enriko D Klootwijk[2#], Joerg Reinders[3#], Edgar A Otto[4#], Mario Milani[5], Carsten Broeker[1], Chris Laing[2], Julia Wiesner[1], Sulochana Devi[6], Weibin Zhou[6], Roland Schmitt[1], Ines Tegtmeier[1], Christina Sterner[1], Hannes Doellerer[1], Kathrin Renner[7], Peter J Oefner[3], Katja Dettmer[3], Johann M Simbuerger[3], Ralph Witzgall[8], Horia C Stanescu[2], Simona Dumitriu[2], Daniela Iancu[2], Vaksha Patel[2], Monika Mozere[2], Mehmet Tekman[2], Graciana Jaureguiberry[2], Naomi Issler[2], Anne Kesselheim[2], Stephen B Walsh[2], Daniel P Gale[2], Alexander J Howie[2], Joana R Martins[9], Andrew M Hall[9], Michael Kasgharian[10], Kevin O'Brien[11], Carlos R Ferreira[11], Paldeep S Atwal[12], Mahim Jain[13], Alexander Hammers[14], Geoffrey Charles-Edwards[15], Chi-Un Choe[16], Dirk Isbrandt[17], Alberto Cebrian-Serrano[18], Ben Davies[18], Richard N Sandford[19], Christopher Pugh[20], David S Konecki[21], Sue Povey[22], Detlef Bockenhauer[2], Uta Lichter-Konecki[23], William A Gahl[11#], Robert J Unwin[2#], Richard Warth[1#*], Robert Kleta[2#*]

# *Contributed equally*
* *Corresponding authors*

[1]Medical Cell Biology, University Regensburg, Germany.
[2]Centre for Nephrology, University College London, UK.
[3]Institute of Functional Genomics, University Regensburg, Germany.
[4]Division of Nephrology, University of Michigan, Ann Arbor, MI, USA.
[5]CNR-Biophysics Institute, Milan, Italy.
[6]Dept. of Ped. and Comm. Dis., University of Michigan, Ann Arbor, MI, USA.
[7]Department of Internal Medicine III, University Regensburg, Germany.
[8]Molecular and Cellular Anatomy, University Regensburg, Germany.
[9]Institute of Anatomy, University of Zurich, Switzerland.
[10]Department of Pathology, Yale University, New Haven, CT, USA.
[11]NHGRI, NIH, Bethesda, MD, USA.
[12]Mayo Clinic, Jacksonville, FL, USA.
[13]Kennedy Krieger Institute, Baltimore, MD, USA.
[14]King's College London & Guy's and St Thomas' PET Centre, London, UK.
[15]Medical Physics, Guy's & St Thomas' NHS Foundation Trust, London, UK.
[16]Department of Neurology, University Hamburg, Germany.
[17]DZNE RG Experimental Neurophysiology, University of Cologne, Germany.
[18]Wellcome Trust Centre for Human Genetics, University of Oxford, UK.
[19]Department of Medical Genetics, University of Cambridge, UK.
[20]Nuffield Dept. Medicine, University of Oxford, UK.
[21]GeneDX, Gaithersburg, MD, USA.
[22]Genetics, Evolution and Environment, University College London, UK.
[23]Division of Medical Genetics, University of Pittsburgh, PA, USA.

Running title: Role of GATM in kidney failure

Word count abstract: 229
Word count text: 3247 (including abstract, significance statement, and main text)

Corresponding authors:

Richard Warth, MD
Medical Cell Biology
University of Regensburg
Universitaetsstr. 31,
93053 Regensburg, Germany
Phone: +49-941-9432894
Fax: +49-941-9432896
Email: richard.warth@ur.de

Robert Kleta, MD, PhD, FASN
University College London
Centre for Nephrology
Royal Free Hospital
London NW3 2PF, UK
Phone: +44-20-7317 7554
Fax: +44-20-7472 6476
Email: r.kleta@ucl.ac.uk

Key words: AGAT, mitochondriopathy, tubulopathy, protein deposits, fibrosis

1

Significance statement:

This manuscript describes a novel mechanism of renal tubular damage and chronic kidney disease involving the formation of unique intramitochondrial protein aggregates. The disease results from monoallelic mutations in the gene "glycine amidinotransferase" (GATM), a proximal tubular enzyme in the creatine biosynthetic pathway. All disease related GATM mutations create an additional interaction interface within the GATM protein, promoting its linear aggregation. Aggregates-containing mitochondria in proximal tubular cells are associated with elevated production of reactive oxygen species, initiation of an inflammatory response and increased cell death. These data establish a link between intramitochondrial GATM aggregates, renal Fanconi syndrome and chronic kidney disease.

Abstract:

Background: For many cases of kidney failure, the cause and underlying defect remain unknown. Here we describe a novel mechanism of renal Fanconi syndrome and chronic kidney disease involving the formation of unique intramitochondrial protein aggregates.

Methods: We clinically and genetically characterized members of five families with autosomal dominant renal Fanconi syndrome and kidney failure. We performed genome-wide linkage analysis, sequencing and expression studies in kidney biopsies and renal cells, along with knockout mouse studies and evaluations of mitochondrial morphology and function. Structural studies examined the effects of recognized mutations.

Results: The renal disease in our patients resulted from monoallelic mutations in the gene "glycine amidinotransferase" (GATM), a renal proximal tubular enzyme in the creatine biosynthetic pathway that is otherwise associated with a recessive disorder of creatine deficiency. The particular GATM mutations, identified in 28 members of five families with progressive kidney failure, created an additional interaction interface within the GATM protein, promoting its linear aggregation. Aggregates-containing mitochondria were elongated and associated with increased ROS production, activation of the NLRP3 inflammasome, enhanced expression of the profibrotic cytokine IL-18 and increased cell death.

Conclusion: In this novel genetic disorder, fully penetrant heterozygous missense mutations in *GATM* trigger intramitochondrial fibrillary deposition of GATM and lead to elongated and abnormal mitochondria. We speculate that this renal proximal tubular mitochondrial pathology initiates a response from the inflammasome with subsequent development of kidney fibrosis.

1
2
3
4
5
6
7
8
9
10
11
12
13
14
15
16
17
18
19
20
21
22
23
24
25
26
27
28
29
30
31
32
33
34
35
36
37
38
39
40
41
42
43
44
45
46
47
48
49
50
51
52
53
54
55
56
57
58
59
60

Introduction:

"Chronic kidney disease" (CKD) is a worldwide health problem and comprises heterogeneous disorders affecting kidney structure and function.[1] The underlying pathogenesis is complex and, in many cases, involves genetic predisposition.

Here, we describe in five extended families a novel form of autosomal dominant kidney disease. The disease is characterized by renal tubular Fanconi syndrome early in life followed by progression to renal glomerular failure in mid-adulthood. All our patients show monoallelic mutations in the gene GATM that create an additional protein-protein interaction surface at which the protein multimerizes leading to large mitochondrial protein aggregates. The appearance of these aggregates was paralleled by increased production of reactive oxygen species, inflammatory signals, cell death, and renal fibrosis. This new disease expands the gamut of etiologies of tubuloglomerular disease.

4

Methods:

Full details of the methods can be found in the Supplemental Data.

Patients

Members of two families were admitted to the NIH Clinical Center and enrolled in clinical protocols 1-HG-0106 or 76-HG-0238. Three further families were evaluated in Cambridge, Oxford, and London. All participating individuals or their parents gave written, informed consent. All investigations, including genetic studies, were approved by the respective Institutional Review Boards and conducted according to the principles of the Declaration of Helsinki.

The diagnosis of renal Fanconi syndrome and kidney failure was established by routine laboratory investigations of urine and blood samples. Clinical details concerning four of these five families have been published previously.[2-10] Kidney samples were acquired from two affected individuals. One patient was biopsied at age 21, another patient died at age of 65 due to end stage renal failure and the kidney was studied at autopsy. Electron microscopic studies and histological stainings were performed using established procedures.[11] One affected and one unaffected adult underwent brain 1H-NMR spectroscopy utilizing standard diagnostic procedures.[12]

Genetic studies

We previously linked the locus for this trait in an extended US family (Figure 1A, Family 1) to a region on chromosome 15q.[13] To prove linkage to the same locus, we performed additional linkage studies in our other families showing the same trait. To this end, DNA was isolated from whole blood using standard procedures and was genotyped with 2000 highly polymorphic STS markers by deCODE Genetics (Iceland) for families 3, 4, 5 or commercially available SNP chips (Affymetrix) for family 2 (Figure 1A). Multipoint parametric linkage

5

analysis was performed using established procedures for families 2-5.[12] Initial gene discovery was performed by either targeted capture and next generation sequencing (The Eastern Sequence and Informatics Hub, University of Cambridge, UK) or whole exome sequencing (SeqWright, Inc, Houston, TX, USA) in six affected individuals from four of our families. Recognized sequence variants within the linked region were examined for segregation in all available affected and unaffected family members and confirmed by Sanger sequencing. Observed novel sequence variants were assessed for uniqueness and evolutionary conservation in various species. Public databases (dbSNP, 1000 Genomes, exome database) were also interrogated.

Renal proximal tubular cell model and kidney imaging

A permanently transfected, inducible renal proximal tubular cell line derived from LLC-PK1 cells was created for each patient GATM mutation using recombinant technology. LLC-PK1 cells are an established model and reliably express many properties of the renal proximal tubule.[11] For *in-situ* immunostaining, subcellular studies, metabolic studies, expression studies and electron microscopy, cells and tissues were prepared and investigated using established procedures. Specifically, the renal and intracellular localization of GATM was studied. Changes in expression of relevant genes were studied using established real-time PCR technology.

***Gatm* knockout mice**

All animal experiments were performed according to the guidelines for the care and use of laboratory animals published by the US National Institutes of Health and were approved by the local councils for animal care according to the German law for animal care. We previously generated *Gatm* knockout mice to study the biochemical function of this mitochondrial protein.[14] Mutant mice were viable, without detectable gross phenotypic

6

defects, but dystrophic. Urinary metabolites were assessed in knockout and control mice using established analytic procedures.

Structural studies

To test the hypothesis of mutation-mediated aggregation of GATM, we performed molecular dynamics simulations on the wildtype monomer and on the four mutants. Modelling of possible protein-protein interaction surfaces (GRAMM-X; vakser.bioinformatics.ku.edu/resources/gramm/grammx/) started with the structure of the wildtype monomer (pdb: 1JDW).

Statistical methods

Data are presented as the mean ± SEM (standard error of the mean) and were analyzed using one-way ANOVA or Student's t-test if not specified otherwise. For all analysis, if not stated otherwise, a p-value of 0.05 was accepted to indicate statistical significance. Statistical analysis was performed using GraphPad Prism 5, OriginPro, and SPSS software.

7

Results:

Clinical studies

All affected individuals from five extended families (Figure 1A) exhibited an autosomal dominant form of "chronic kidney disease" (CKD). During childhood, all patients developed a renal Fanconi syndrome with glucosuria, hyperphosphaturia, generalized hyperaminoaciduria, low molecular weight proteinuria and metabolic acidosis, but without debilitating rickets or bone deformities. As an example, at age 18 months the youngest affected child studied exhibited laboratory findings typical of renal Fanconi syndrome but no glomerular compromise (Supplemental Table S1). During late adolescence or adulthood, increased plasma creatinine became apparent and patients developed renal fibrosis and kidney failure, with the need for transplant or dialysis in the third to sixth decade of life. A graph illustrating the decline in kidney function in relation to age is shown in Supplemental Figure S1. Premature deaths due to compromised glomerular kidney function occurred in several families. No extra-renal clinical findings were noted.

Genetic analyses

In all six affected individuals initially studied, sequencing of all genes within the linked locus on chromosome 15 (Figure 1B) showed mutations in a single gene, identified as "glycine amidinotransferase", GATM. Subsequent sequencing of all 28 clinically affected individuals showed each had one heterozygous missense mutation in GATM. We identified four previously unreported heterozygous missense mutations of evolutionary conserved amino acid residues in GATM (c.958C>T, p.P320S; c.1006A>G, p.T336A; c.1007C>T, p.T336I; c.1022C>T, p.P341L). In each family, one variant segregated with the disorder and was fully penetrant. None of the unaffected family members carried any of these GATM mutations. One family showed a *de novo* heterozygous mutation in affected offspring confirmed by haplotype analysis, which was passed on to the next generation (Figure 1A, Family 4).

8

Histological examinations

Patients' biopsies showed the morphological correlate of kidney fibrosis on routine staining (Figure 1 C-F). In normal kidneys, GATM was found in mitochondria of proximal tubules, particularly in the early segments.[15] In a patient's kidney biopsy, electron microscopy and GATM-specific immunogold staining of renal proximal tubules revealed drastically enlarged mitochondria containing pathological GATM protein aggregates (Figure 2 A-C).

To further explore the pathophysiological mechanisms of this particular mitochondrial phenotype, we over-expressed wildtype or mutant GATM in a renal proximal tubule cell line, LLC-PK1. Normal mitochondrial morphology was observed in cells expressing wildtype GATM, but abnormal and elongated mitochondria were observed in the cells expressing the GATM T336A mutant (Figure 2D-F). Similar findings were present in cells transfected with GATM mutants T336I, P341L, and P320S (unpublished data). Immunogold electron microscopy of cells over-expressing mutant GATM demonstrated drastically enlarged mitochondria containing GATM-positive fibrillary aggregates, similar to the deposits observed in proximal tubules of patients' biopsies (Figure 2G-I).

Structural studies

We performed *in silico* structural studies of GATM, which contains ten X-ray crystallographic structures in the protein data bank.[16] The 423-amino acid GATM protein is built around a central core formed by five antiparallel beta sheets (B1-B5) disposed around a five-fold axis of symmetry. Such a structure is potentially prone to protein-protein aggregation due to the presence of the five solvent-exposed beta sheets. In addition to the domain of five-fold symmetry, the GATM protein hosts one additional domain composed of four alpha helices and a beta hairpin involved in formation of the wildtype dimer. Assembly of the physiological GATM dimer involves the two facing beta sheets (B2) disposed in parallel with an angle of

9

approximately 45° with respect to each other, harboring the catalytic enzymatic activity domain (Figure 2J, K).

The four disease-related mutations involve three amino acids conserved through evolution, i.e., Pro320, Pro341, and Thr336. All three are located on the surface around sheet B4, which is located opposite to the B2 surface (Figure 2K, L). Thus, these mutations could impair the proper folding of the B4 surface. In fact, structure simulations of these four GATM mutants predicted increased mobility of the same region for each of them, predisposing the mutated B4 region to form an additional interaction site. Specifically, the presence of two opposite dimerization surfaces, B2 and B4, would support the formation of linear multimers, with each mutant GATM monomer linked to two protein partners by two dimerization interfaces, i.e. the existing "physiological" "B2-B2" and the "de novo" pathological "B4-B4" interface (Figure 2M).

Gatm^{-/-} mouse studies

We employed *Gatm*^{-/-} mice to determine whether mitochondrial *GATM* haploinsufficiency (i.e. decreased GATM activity) was likely to have caused our families' renal Fanconi syndrome. No aminoaciduria and no glucosuria was observed in these mice (Supplemental Figure S2), indicating that lack of GATM did not significantly affect renal proximal tubular function. Rather, we propose that mutant GATM proteins within mitochondria trigger a pathological cascade inside and outside the proximal tubules, resulting in our patients' signs and symptoms.

Intramitochondrial deposits impair mitochondrial degradation and elicit an inflammatory response

In a next set of experiments we investigated mitochondrial turnover in cells over-expressing mutant GATM. Electron micrographs of these cells indicated that the fibrillary GATM deposits

10

might impair mitochondrial fission and, thus, mitochondrial degradation (Figure 2I). Indeed, over-expression of mutant GATM led to a reduced mitochondrial turnover rate in our cell model. This was evidenced by the presence of GATM-positive enlarged mitochondria even 8 weeks after induction of GATM T336A expression was discontinued (Figure 3A-H).

Furthermore, we explored possible links between mitochondrial GATM protein deposits and pathways inducing tubular damage and renal fibrosis. The mitochondrial phenotype in our cell model was associated with an increased production of reactive oxygen species (ROS) (Figure 3I). Excess ROS generation leads to oxidative stress and triggers - in concert with other factors - the inflammasome.[17-20] In fact, LLC-PK1 cells carrying mitochondrial GATM deposits showed significantly elevated mRNA expression of both the inflammasome component NLRP3 and Interleukin 18 (IL-18), a cytokine known to promote renal fibrosis (Figure 3J, K).[21, 22] IL-18 protein was also elevated as measured by ELISA (Figure 3L). Moreover, those cells exhibited increased fibronectin and smooth muscle actin mRNA levels (Figure 4A, B) as well as an increased rate of cell death (Figure 4C, D). These findings strongly suggest that mitochondrial GATM aggregates led to activation of components of the inflammasome and release of profibrotic factors, thereby providing a plausible pathogenic link between heterozygous GATM mutations, kidney fibrosis and renal failure.

Potential treatment

Since mutant GATM protein resulted in pathogenic intramitochondrial deposits in renal proximal tubular cells, we investigated means to reduce GATM production. GATM expression was reported to be negatively feedback regulated by creatine in rats,[23] so we supplemented wildtype mice with 1% creatine in their drinking water for 1 week. This protocol reduced renal GATM mRNA expression by 27% and GATM protein by 58% (Figure 4E, F), corroborating previous findings.[23] Hence, creatine supplementation could serve as an

11

intervention to suppress the endogenous production of mutated GATM protein and to retard the formation of deleterious mitochondrial deposits.

Discussion

"Chronic kidney disease" (CKD) affects 8-16% of the adult population and comprises heterogeneous disorders of unknown etiology affecting kidney structure and function.[1, 24, 25] Here, we provide genetic, histological, cell biological, and structural evidence for the association between monoallelic *GATM* mutations and a genetic disorder characterized by renal Fanconi syndrome and progressive kidney failure.

GATM encodes the mitochondrial enzyme "glycine amidinotransferase" ("L-arginine:glycine amidinotransferase", also known as *AGAT*), which catalyzes the transfer of a guanidino group from L-arginine to glycine, resulting in guanidinoacetic acid, the immediate precursor of creatine.[16, 26, 27] *GATM* is expressed most prominently in kidney, liver, pancreas and brain. Recessive loss-of-function mutations of *GATM* result in "cerebral creatine deficiency syndrome", a rare inborn error of creatine synthesis characterized by severe neurological impairment.[12, 28] A *Gatm*^{-/-} mouse model also showed neurological symptoms caused by creatine deficiency,[14] but had normal kidney function (Supplemental Figure S2). In contrast to patients with "cerebral creatine deficiency syndrome", none of our patients showed extra-renal symptoms. The one patient studied by brain ^{1}H-NMR spectroscopy had a normal creatine peak (Supplemental Figure S3), indicating that the disorder in our patients was not related to creatine deficiency.

Histological examinations of patients' kidney biopsies revealed a dramatic mitochondrial phenotype associated with GATM mutations. Mitochondria of proximal tubular cells were drastically enlarged and filled with filament-like deposits. This phenotype was also observed in a LLC-PK1 cell model over-expressing GATM mutants. Immunogold studies on

12

a patient biopsy and LLC-PK1 cells demonstrated that these deposits were composed of mutant GATM protein, and *in silico* structural studies provided an explanation. Heterozygous GATM mutations in a particular region of the enzyme led to the creation of an additional *de novo* interaction surface, causing intramitochondrial "multimeric" aggregation. This gain-of-function effect of the mutations was in line with the dominant inheritance of the disease.

Mitochondrial fission results in smaller mitochondria and, thereby, facilitates removal and degradation of aged mitochondria by mitophagy.[29] Intramitochondrial aggregates of mutant GATM apparently impaired mitochondrial division, leading to pathologically enlarged and aged mitochondria which could no longer be removed by mitophagy. In our LLC-PK1 cell model, mitochondria with GATM deposits were still present even 8 weeks after GATM mRNA expression was discontinued. The long persistence of deposits contrasted with the physiological turnover rate of mitochondria, estimated to be 2-4 weeks.[29] These data suggest that the long fibrillary deposits of mutant GATM, once aggregated, escape cellular degradation, prevent mitochondrial fission and lead to enlarged, aged mitochondria.

Aged mitochondria as well as non-degradable deposits and crystalline structures are known to trigger an inflammatory response and activate the NLRP3 inflammasome.[17, 18, 30-33] In agreement with these reports, the appearance of mutant GATM aggregates in our cell model was paralleled by enhanced inflammatory markers: NLRP3 and its downstream signaling molecule Interleukin 18 (IL-18) were strongly elevated. We also found evidence of increased reactive oxygen species (ROS) production in mutated cells. Mitochondria are a major source of intracellular ROS, and excess ROS generation is known to lead to oxidative stress and trigger the inflammasome, too.[34, 35] In addition, over-expression of mutant GATM led to an increased rate of cell death and enhanced expression of the fibrosis marker fibronectin and smooth muscle actin. In line with this profound *in vitro* cytopathological phenotype, immunofluorescence studies in kidney biopsies from our patients revealed significant interstitial fibrosis with myofibroblasts surrounding renal tubules and thickening of tubular basement membranes, eventually leading to kidney failure.[20, 21, 33]

13

Taken together, we provide evidence that intramitochondrial aggregates consisting of mutated glycine amidinotransferase (GATM) protein are causative for an autosomal dominant form of renal Fanconi syndrome and chronic kidney disease. This finding extends the spectrum of disorders associated with pathological protein aggregates beyond neurodegenerative disorders such as Alzheimer's disease. The disease also illustrates the critical role mitochondria can play in initiating devastating profibrotic signaling cascades. This may have implications for understanding the pathophysiology of chronic kidney disease. An association of genetic variation in the GATM gene to plasma creatinine levels was previously suggested by genome-wide association studies.[36-38]

Cohorts of patients with kidney failure or renal insufficiency deserve up-to-date genetic diagnostic procedures, with attention to *de novo* mutations. Sequencing of GATM should be considered in patients with kidney failure, particularly adults with or without familial occurrence. Moreover, kidney biopsies that do not yield a diagnosis based upon standard histology should be considered for ultrastructural analysis, with consideration of tubular pathology rather than an evaluation limited to the glomerulus and interstitium. Finally, for patients with autosomal dominant GATM mutations, only 50% of the GATM protein is abnormal, and biosynthesis of creatine is negatively feedback regulated by its product.[23] Hence, creatine supplementation could serve as a pharmacological intervention to suppress the endogenous production of mutated GATM protein, which triggers the cascade leading ultimately to kidney fibrosis and failure.

Author contributions:

All authors together generated and gathered the patient, animal, genetic and molecular data and analyzed the data. William A Gahl, Robert J Unwin, Richard Warth, and Robert Kleta (overall responsible) vouch for the data and the analysis. All authors helped writing the paper, and all together decided to publish this paper.

14

15

References:

1. Jha, V, Garcia-Garcia, G, Iseki, K, Li, Z, Naicker, S, Plattner, B, et al.: Chronic kidney disease: global dimension and perspectives. *Lancet,* 382**:** 260-272, 2013.
2. Dent, CE, Harris, H: The genetics of cystinuria. *Ann Eugen,* 16**:** 60-87, 1951.
3. Luder, J, Sheldon, W: A familial tubular absorption defect of glucose and amino acids. *Arch Dis Child,* 30**:** 160-164, 1955.
4. Sheldon, W, Luder, J, Webb, B: A familial tubular absorption defect of glucose and amino acids. *Arch Dis Child,* 36**:** 90-95, 1961.
5. Smith, R, Lindenbaum, RH, Walton, RJ: Hypophosphataemic osteomalacia and Fanconi syndrome of adult onset with dominant inheritance. Possible relationship with diabetes mellitus. *Q J Med,* 45**:** 387-400, 1976.
6. Brenton, DP, Isenberg, DA, Cusworth, DC, Garrod, P, Krywawych, S, Stamp, TC: The adult presenting idiopathic Fanconi syndrome. *J Inherit Metab Dis,* 4**:** 211-215, 1981.
7. Patrick, A, Cameron, JS, Ogg, CS: A family with a dominant form of idiopathic Fanconi syndrome leading to renal failure in adult life. *Clin Nephrol,* 16**:** 289-292, 1981.
8. Wen, SF, Friedman, AL, Oberley, TD: Two case studies from a family with primary Fanconi syndrome. *Am J Kidney Dis,* 13**:** 240-246, 1989.
9. Long, WS, Seashore, MR, Siegel, NJ, Bia, MJ: Idiopathic Fanconi syndrome with progressive renal failure: a case report and discussion. *Yale J Biol Med,* 63**:** 15-28, 1990.
10. Harrison, NA, Bateman, JM, Ledingham, JG, Smith, R: Renal failure in adult onset hypophosphatemic osteomalacia with Fanconi syndrome: a family study and review of the literature. *Clin Nephrol,* 35**:** 148-150, 1991.
11. Klootwijk, ED, Reichold, M, Helip-Wooley, A, Tolaymat, A, Broeker, C, Robinette, SL, et al.: Mistargeting of peroxisomal EHHADH and inherited renal Fanconi's syndrome. *N Engl J Med,* 370**:** 129-138, 2014.
12. Joncquel-Chevalier, CM, Voicu, PM, Fontaine, M, Dessein, AF, Porchet, N, Mention-Mulliez, K, et al.: Creatine biosynthesis and transport in health and disease. *Biochimie,* 119**:** 146-165, 2015.
13. Lichter-Konecki, U, Broman, KW, Blau, EB, Konecki, DS: Genetic and physical mapping of the locus for autosomal dominant renal Fanconi syndrome, on chromosome 15q15.3. *Am J Hum Genet,* 68**:** 264-268, 2001.
14. Choe, CU, Nabuurs, C, Stockebrand, MC, Neu, A, Nunes, P, Morellini, F, et al.: L-arginine:glycine amidinotransferase deficiency protects from metabolic syndrome. *Hum Mol Genet,* 22**:** 110-123, 2013.
15. McGuire, DM, Gross, MD, Elde, RP, van Pilsum, JF: Localization of L-arginine-glycine amidinotransferase protein in rat tissues by immunofluorescence microscopy. *J Histochem Cytochem,* 34**:** 429-435, 1986.
16. Humm, A, Fritsche, E, Steinbacher, S, Huber, R: Crystal structure and mechanism of human L-arginine:glycine amidinotransferase: a mitochondrial enzyme involved in creatine biosynthesis. *EMBO J,* 16**:** 3373-3385, 1997.
17. Halle, A, Hornung, V, Petzold, GC, Stewart, CR, Monks, BG, Reinheckel, T, et al.: The NALP3 inflammasome is involved in the innate immune response to amyloid-beta. *Nat Immunol,* 9**:** 857-865, 2008.
18. Dostert, C, Petrilli, V, Van, BR, Steele, C, Mossman, BT, Tschopp, J: Innate immune activation through Nalp3 inflammasome sensing of asbestos and silica. *Science,* 320**:** 674-677, 2008.
19. Vilaysane, A, Chun, J, Seamone, ME, Wang, W, Chin, R, Hirota, S, et al.: The NLRP3 inflammasome promotes renal inflammation and contributes to CKD. *J Am Soc Nephrol,* 21**:** 1732-1744, 2010.
20. Anders, HJ, Schaefer, L: Beyond tissue injury-damage-associated molecular patterns, toll-like receptors, and inflammasomes also drive regeneration and fibrosis. *J Am Soc Nephrol,* 25**:** 1387-1400, 2014.

21. Liang, D, Liu, HF, Yao, CW, Liu, HY, Huang-Fu, CM, Chen, XW, et al.: Effects of interleukin 18 on injury and activation of human proximal tubular epithelial cells. *Nephrology (Carlton),* 12**:** 53-61, 2007.

22. Bani-Hani, AH, Leslie, JA, Asanuma, H, Dinarello, CA, Campbell, MT, Meldrum, DR, et al.: IL-18 neutralization ameliorates obstruction-induced epithelial-mesenchymal transition and renal fibrosis. *Kidney Int,* 76**:** 500-511, 2009.

23. McGuire, DM, Gross, MD, Van Pilsum, JF, Towle, HC: Repression of rat kidney L-arginine:glycine amidinotransferase synthesis by creatine at a pretranslational level. *J Biol Chem,* 259**:** 12034-12038, 1984.

24. Zhou, D, Liu, Y: Renal fibrosis in 2015: Understanding the mechanisms of kidney fibrosis. *Nat Rev Nephrol,* 12**:** 68-70, 2016.

25. Bohle, A, Mackensen-Haen, S, von, GH: Significance of tubulointerstitial changes in the renal cortex for the excretory function and concentration ability of the kidney: a morphometric contribution. *Am J Nephrol,* 7**:** 421-433, 1987.

26. Guthmiller, P, Van Pilsum, JF, Boen, JR, McGuire, DM: Cloning and sequencing of rat kidney L-arginine:glycine amidinotransferase. Studies on the mechanism of regulation by growth hormone and creatine. *J Biol Chem,* 269**:** 17556-17560, 1994.

27. Wyss, M, Kaddurah-Daouk, R: Creatine and creatinine metabolism. *Physiol Rev,* 80**:** 1107-1213, 2000.

28. Item, CB, Stockler-Ipsiroglu, S, Stromberger, C, Muhl, A, Alessandri, MG, Bianchi, MC, et al.: Arginine:glycine amidinotransferase deficiency: the third inborn error of creatine metabolism in humans. *Am J Hum Genet,* 69**:** 1127-1133, 2001.

29. Terman, A, Kurz, T, Navratil, M, Arriaga, EA, Brunk, UT: Mitochondrial turnover and aging of long-lived postmitotic cells: the mitochondrial-lysosomal axis theory of aging. *Antioxid Redox Signal,* 12**:** 503-535, 2010.

30. Nakahira, K, Haspel, JA, Rathinam, VA, Lee, SJ, Dolinay, T, Lam, HC, et al.: Autophagy proteins regulate innate immune responses by inhibiting the release of mitochondrial DNA mediated by the NALP3 inflammasome. *Nat Immunol,* 12**:** 222-230, 2011.

31. Duewell, P, Kono, H, Rayner, KJ, Sirois, CM, Vladimer, G, Bauernfeind, FG, et al.: NLRP3 inflammasomes are required for atherogenesis and activated by cholesterol crystals. *Nature,* 464**:** 1357-1361, 2010.

32. Knauf, F, Asplin, JR, Granja, I, Schmidt, IM, Moeckel, GW, David, RJ, et al.: NALP3-mediated inflammation is a principal cause of progressive renal failure in oxalate nephropathy. *Kidney Int,* 84**:** 895-901, 2013.

33. Mulay, SR, Kulkarni, OP, Rupanagudi, KV, Migliorini, A, Darisipudi, MN, Vilaysane, A, et al.: Calcium oxalate crystals induce renal inflammation by NLRP3-mediated IL-1beta secretion. *J Clin Invest,* 123**:** 236-246, 2013.

34. Fougeray, S, Pallet, N: Mechanisms and biological functions of autophagy in diseased and ageing kidneys. *Nat Rev Nephrol,* 11**:** 34-45, 2015.

35. Abais, JM, Xia, M, Zhang, Y, Boini, KM, Li, PL: Redox regulation of NLRP3 inflammasomes: ROS as trigger or effector? *Antioxid Redox Signal,* 22**:** 1111-1129, 2015.

36. Kottgen, A, Glazer, NL, Dehghan, A, Hwang, SJ, Katz, R, Li, M, et al.: Multiple loci associated with indices of renal function and chronic kidney disease. *Nat Genet,* 41**:** 712-717, 2009.

37. Park, H, Kim, HJ, Lee, S, Yoo, YJ, Ju, YS, Lee, JE, et al.: A family-based association study after genome-wide linkage analysis identified two genetic loci for renal function in a Mongolian population. *Kidney Int,* 83**:** 285-292, 2013.

38. Pattaro, C, Teumer, A, Gorski, M, Chu, AY, Li, M, Mijatovic, V, et al.: Genetic associations at 53 loci highlight cell types and biological pathways relevant for kidney function. *Nat Commun,* 7**:** 10023, 2016.
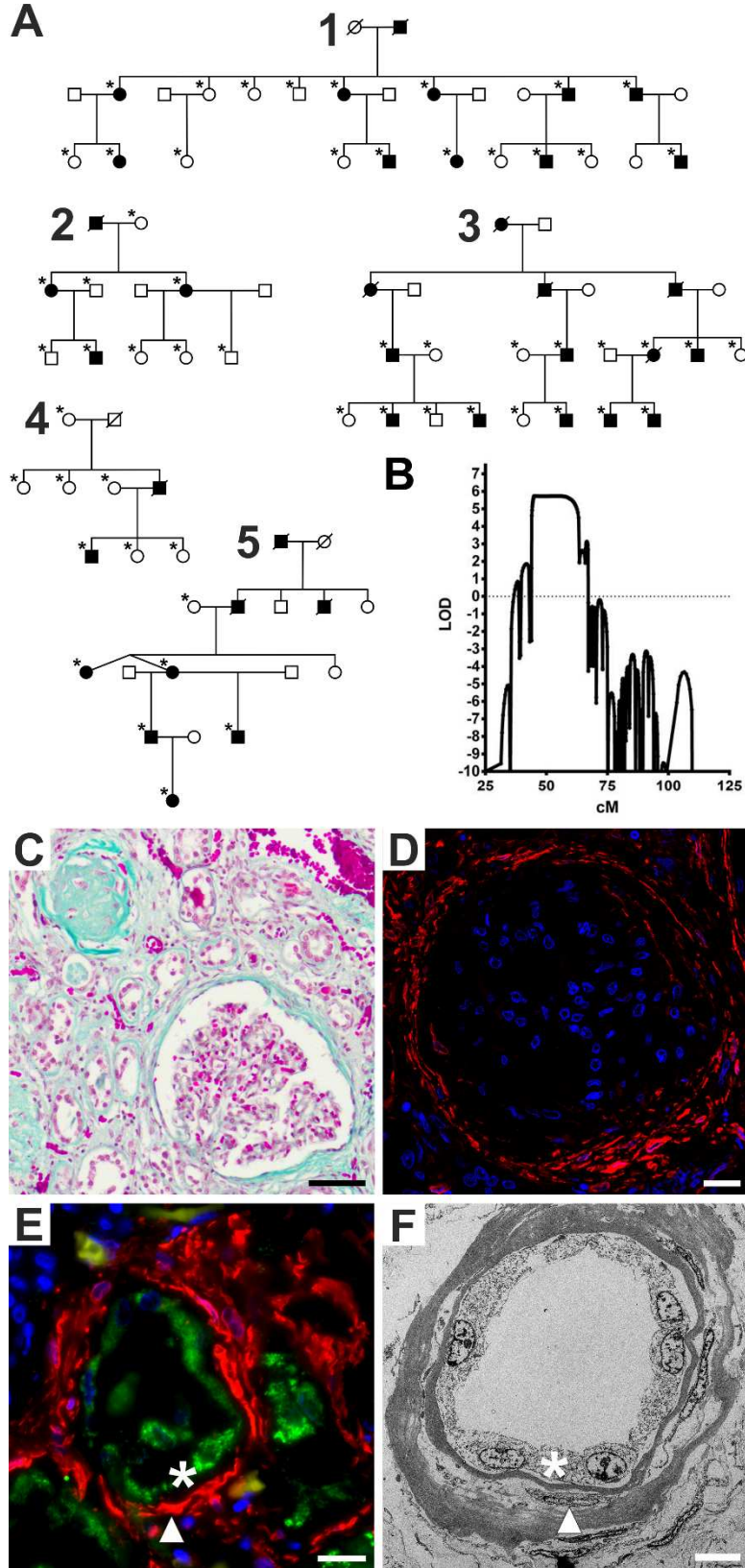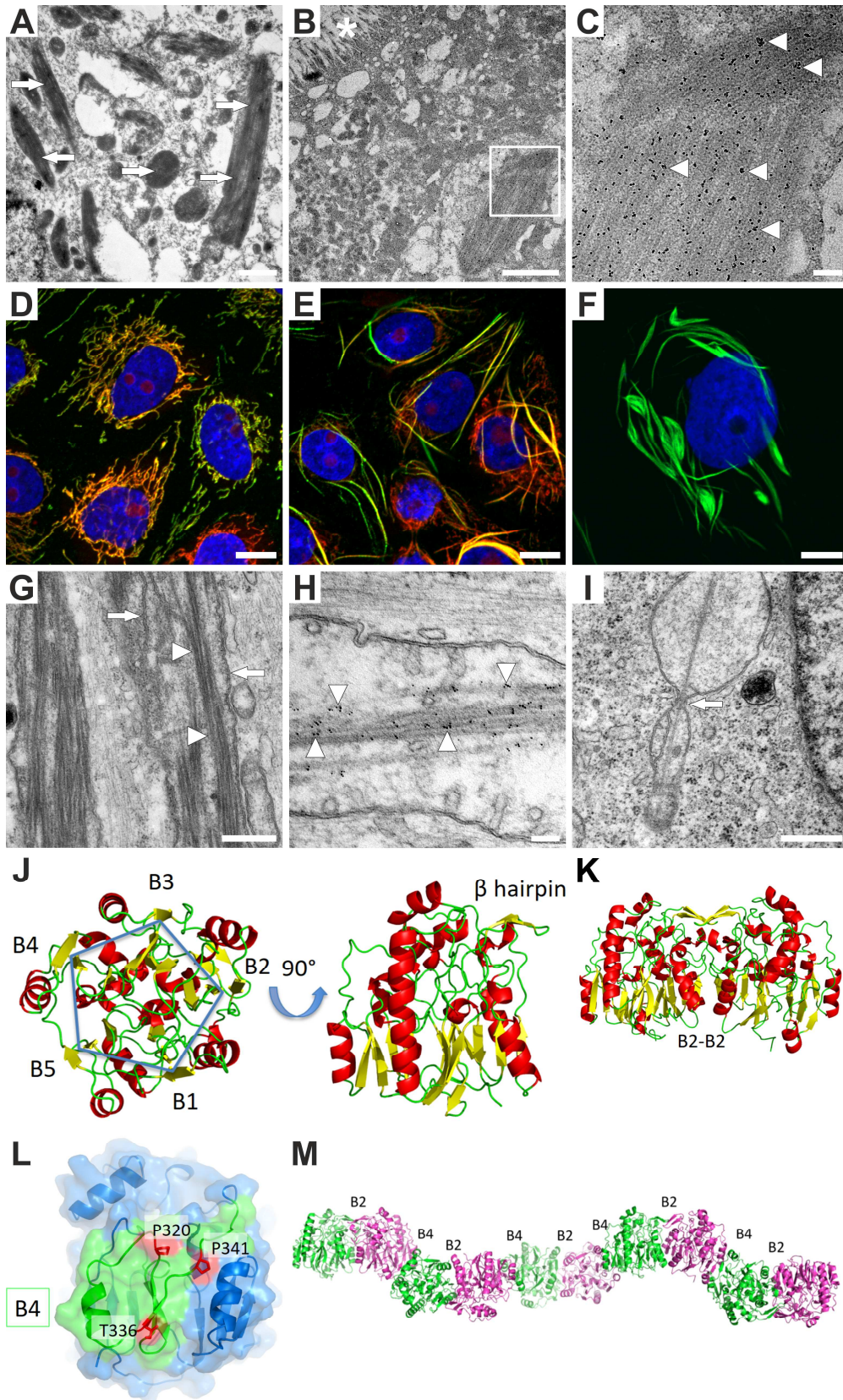
Figures:

Figure 1

Figure 2

Figure 3

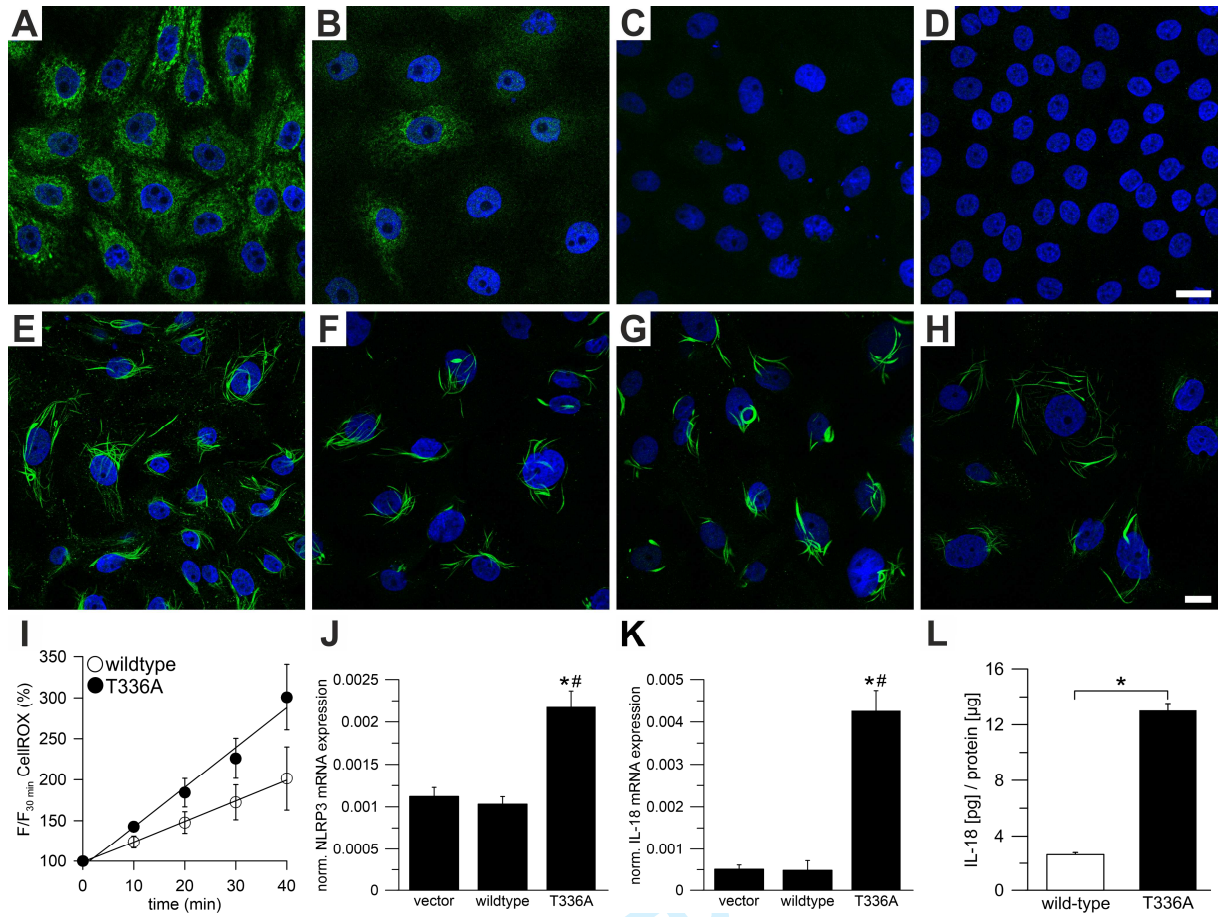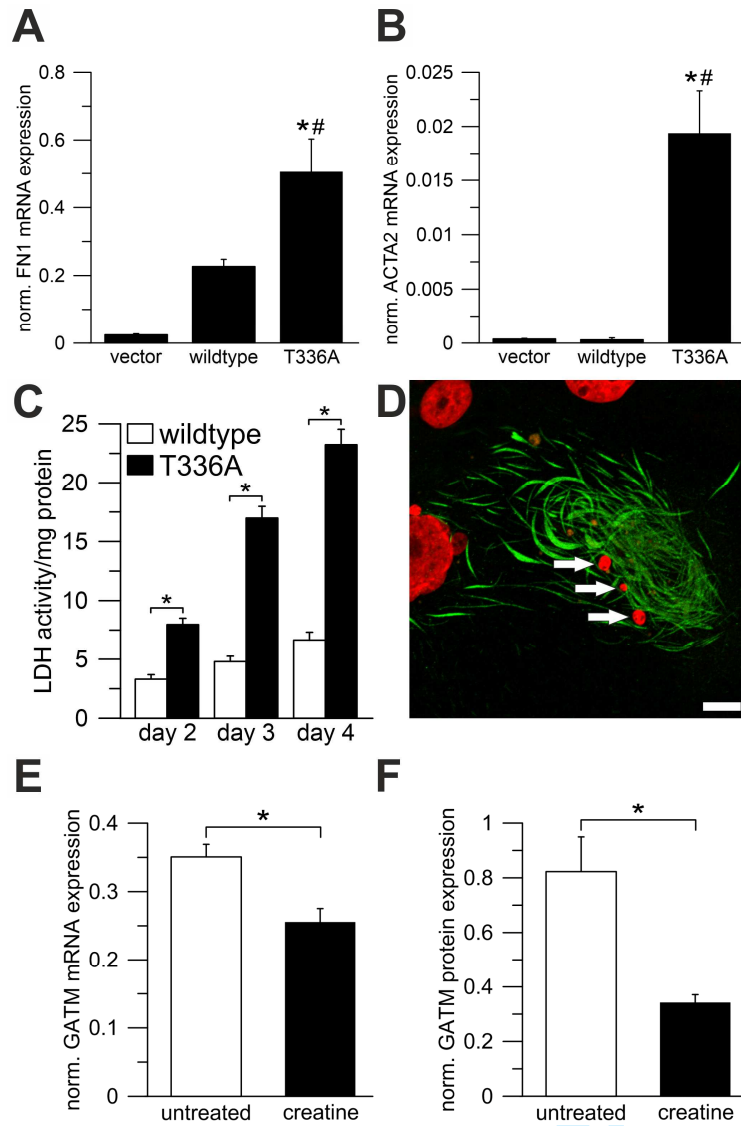**Figure 4**

Figure legends:

Figure 1: Genetic analysis and kidney histology

(A) Pedigrees of families with renal Fanconi syndrome and kidney failure. Squares indicate males and circles females; a filled symbol indicates that the person is affected; deceased individuals are drawn with a diagonal line through the symbol. An asterisk indicates that the person contributed to linkage and sequencing studies. Note *de novo* "appearance" of the disease in family 4.

(B) Multipoint parametric linkage analysis for families 3, 4, 5 for chromosome 15. The y-axis shows the LOD score, and the x-axis gives the genetic distance in cM. Note significant linkage (LOD score > 3) in the region of 40 - 60 cM.

(C) Masson-Goldner staining of a renal Fanconi and kidney failure patient's post mortem kidney specimen. Connective tissue is stained light green. This specimen shows the highly fibrotic terminal kidney morphology of the disease. The cortex is shrunken and contains very few proximal tubules. Most glomeruli are atrophic and fibrotic (upper left corner), some appear intact (lower right corner). Scale bar: 50 µm.

(D) Immunofluorescence of same specimen as in (C). α-smooth muscle actin (a marker for myofibroblasts) stains red, and nuclei blue. The Bowman capsule of the glomerulus contains myofibroblasts (red), which suggests that the kidney damage is not restricted to proximal tubules during the final stage of the disease. Scale bar: 20 µm.

(E) Immunofluorescence of same specimen as in (C). GATM stains green, α-smooth muscle actin (a marker for myofibroblasts) red, and nuclei blue. The picture shows a proximal tubule with GATM positive epithelium (asterisk). Several layers of myofibroblasts (arrowhead) surround the tubule. Scale bar: 20 µm.

(F) Electron microscopy of same specimen as in (C). Most tubules show an extremely thick basal membrane containing myofibroblasts (arrowhead). Tubular epithelium is marked by an asterisk. Scale bar: 7 μm.

Figure 2: Mitochondrial morphology and structural analysis

(A) Electron microscopy of a proximal tubular cell from a patient's biopsy showing giant mitochondria with deposits (arrows). Scale bar: 1000 nm.

(B) GATM-immunogold electron microscopy of a proximal tubular cell with an enlarged, filament-containing mitochondrion from a patient's biopsy. Asterisk indicates proximal tubule brush border membrane. Scale bar: 2 μm.

(C) Higher magnification of (B) (white square). Note packed linear deposits with 6 nm GATM-specific gold particles attached (arrow heads). Scale bar: 200 nm.

(D) Immunofluorescence of LLC-PK1 renal proximal tubular cells with induced expression (3 days) of wildtype GATM (green). Normal mitochondria in red (mitotracker), nuclei in blue, scale bar: 20 μm.

(E) Immunofluorescence of LLC-PK1 cells with induced expression (3 days) of mutant GATM (T336A, green) and abnormal mitochondria (red). Nuclei in blue, scale bar: 20 μm.

(F) Immunofluorescence of LLC-PK1 cells with induced expression (9 weeks) of mutant GATM (green) causing large deposits. Nucleus in blue, scale bar: 10 μm.

(G) Electron microscopy of an LLC-PK1 cell overexpressing the T336A mutant. Within the mitochondrial matrix, GATM filaments were aligned in a parallel manner (arrow heads). Cristae are marked by arrows, scale bar: 500 nm.

(H) Immunogold electron microscopy of mutant GATM (T336A) in LLC-PK1 cells. Intramitochondrial gold particles attached to linear long aggregates (arrow heads) indicate that GATM comprises these deposits. Scale bar: 100 nm.

23

(I) Electron microscopy of LLC-PK1 cells overexpressing the P341L mutant in LLC-PK1 cells. A GATM filament appears to prevent mitochondrial fission (arrow). Scale bar: 500 nm.

(J) Wildtype GATM in two orientations rotated by 90° around the horizontal axis, colored by secondary structures: yellow β sheets, green loops, and red α helices. In the left orientation, the five-fold symmetry with the five β sheets B1-B5 is visible. In the right orientation, the β hairpin involved in wildtype homo-dimer formation becomes visible.

(K) The wildtype homo-dimer is stabilized by interaction of β sheets B2. (L) Mutated GATM: Surface of the B4 module (green) shows the mutated amino acids in red. Remainder of GATM is blue. Localization of all observed mutations (p.P320S, p.T336A, p.T336I, and p.P341L) on the same surface leads to the appearance of a novel additional interaction site.

(M) Proposed disease mechanism in which the creation of an additional mutation-related novel interaction site in the B4 module can lead to aggregation of GATM multimers instead of the physiological homo-dimer; B2 denotes physiological interaction site forming enzymatically active GATM. B4 denotes additional interaction site opposite the B2 module mediating longitudinal GATM aggregation. Monomers carrying the mutation are shown in green and cyan, respectively.

Figure 3: Giant mitochondria and activation of the NLRP3 inflammasome

(A-D) LLC-PK1 cells, induced with tetracycline for two weeks, over-expressed wildtype GATM. Induction was discontinued to stop further over-expression. GATM was immuno-stained immediately after discontinuing tetracycline (A), after 4 (B), 6 (C) and 8 weeks (D). At week 4, the GATM signal (green) was very faint and at week 6, GATM was no longer detected. Nuclei in blue, scale bar: 20 μm.

(E-H) Protocol as in (A – D), but with LLC-PK1 cells over-expressing the T336A mutant. Within eight weeks, the cells were not able to degrade GATM deposits and giant mitochondria. Scale bar: 20 μm.

24

(I) Live-cell-imaging of mitochondrial reactive oxygen species (ROS) production in LLC-PK1 cells over-expressing wildtype GATM (n = 6) or the T336A mutant (n = 6). ROS production rate was measured with the mitochondrial-targeted superoxide probe CellROX Deep Red. The slopes of the linear regression curves were significantly different (ANCOVA; p=0.0065).

(J, K) Realtime PCR in LLC-PK1 vector control cells (vector), cells over-expressing wildtype GATM (wildtype) and the T336A mutant (T336A); n=20 dishes for each group; mean values ± SEM. Values were normalized to β-actin mRNA expression.

(J) Realtime PCR of the inflammasome component NLRP3. * significantly different from vector control cells (ANOVA, Bonferroni test, p<0.001), # significantly different from wildtype GATM expressing cells (p<0.001).

(K) Realtime PCR of the profibrotic cytokine IL-18. * significantly different from vector control cells (ANOVA, Bonferroni test, p<0.001), # significantly different from wildtype GATM expressing cells (p<0.001).

(L) IL-18 ELISA in total cell lysates of LLC-PK1 cells over-expressing wildtype GATM (n = 3) or the T336A mutant (n = 3). Data were normalized to total protein content. Over-expression of the T336A mutant led to increased IL-18 synthesis (unpaired, two-sided t-test p=0.001).

Figure 4: Fibrosis, cell death, and possible therapeutic intervention

(A, B) Realtime PCR in LLC-PK1 vector control cells (vector), cells over-expressing wildtype GATM (wildtype) and the T336A mutant (T336A); n=20 dishes for each group; mean values ± SEM. Values were normalized to β-actin expression. (A) Realtime PCR of fibronectin 1 (FN1), * significantly different from vector control cells (ANOVA, Bonferroni test p<0.001), # significantly different from wildtype GATM expressing cells (p=0.003). Values of vector controls cells were not different from wildtype GATM expressing cells (p=0.0502). (B) Realtime PCR of α smooth muscle actin 2 (ACTA2). * significantly different from vector

25

control cells (ANOVA, Bonferroni test p<0.001), # significantly different from wildtype GATM expressing cells (p<0.001).

(C) Lactate dehydrogenase (LDH) release as a measure of cell death in LLC-PK1 cells over-expressing wildtype GATM (n = 3) or the T336A mutant (n = 3). After induction (3 weeks), the cell medium remained unchanged and samples were taken on day 2, 3, and 4. ANOVA with post-hoc student´s t-tests corrected for multiple testing by the Bonferroni method; p-values were 0.0039 (day 2), <0.0001 (day 3), and <0.0001 (day 4).

(D) Cell death in LLC-PK1 cells over-expressing the T336A mutant (induced for seven weeks). The remains of a dead cell with giant mitochondria (green). The nucleus (red) is fragmented (arrows) indicating cell death. Scale bar: 10 μm.

(E, F) Effect of oral creatine supplementation on Gatm expression. Wildtype mice were supplemented with 1% creatine in their drinking water (n = 4) for one week; control mice received tap water (n = 4). Renal Gatm mRNA and protein expression were determined using realtime PCR (E) and Western blot (F). Creatine supplementation led to a reduction of mRNA and protein expression (unpaired, two-sided t-tests, p=0.013 and p=0.029, respectively). Values normalized to β-actin mRNA or total protein expression.

26

1
2
3
4
5
6
7
8
9
10
11
12
13
14
15
16
17
18
19
20
21
22
23
24
25
26
27
28
29
30
31
32
33
34
35
36
37
38
39
40
41
42
43
44
45
46
47
48
49
50
51
52
53
54
55
56
57
58
59
60

Supplemental Data for

GATM, renal Fanconi syndrome and kidney failure

Markus Reichold[#], Enriko D Klootwijk[#], Joerg Reinders[#], Edgar A Otto, Mario Milani, Carsten Broeker, Chris Laing, Julia Wiesner, Sulochana Devi, Weibin Zhou, Roland Schmitt, Ines Tegtmeier, Christina Sterner, Hannes Doellerer, Kathrin Renner, Peter J Oefner, Katja Dettmer, Johann M Simbuerger, Ralph Witzgall, Horia C Stanescu, Simona Dumitriu, Daniela Iancu, Vaksha Patel, Monika Mozere, Mehmet Tekman, Graciana Jaureguiberry, Naomi Issler, Anne Kesselheim, Stephen B Walsh, Daniel P Gale, Alexander J Howie, Joana R Martins, Andrew M Hall, Michael Kasgharian, Kevin O'Brien, Carlos R Ferreira, Paldeep S Atwal, Mahim Jain, Alexander Hammers, Geoffrey Charles-Edwards, Chi-Un Choe, Dirk Isbrandt, Alberto Cebrian-Serrano, Ben Davies, Richard N Sandford, Christopher Pugh, David S Konecki, Sue Povey, Detlef Bockenhauer, Uta Lichter-Konecki, William A Gahl[#], Robert J Unwin[#], Richard Warth[#]*, Robert Kleta[#]*

[#] *Contributed equally*
* *Corresponding authors*

Table of Contents

1

Supplementary Materials and Methods

<u>^{1}H-NMR creatine spectroscopy</u>

^{1}H-NMR spectroscopy of body fluids shows the majority of proton-containing compounds and therefore can provide an overall view of metabolism.[1] ^{1}H-NMR spectrum provides a characteristic 'fingerprint' of almost all proton-containing metabolites. In these spectra, the spectral parameters chemical shift, spin-spin coupling, and signal intensity are important for body fluid analysis. The peak area or signal intensity of a resonance in a ^{1}H-NMR spectrum is proportional to the number of protons contributing to the signal when appropriate experimental conditions are used. Since the peak area is proportional to the number of protons contributing to the signal, it is also proportional to the concentration of the molecule concerned. Therefore, it is possible to use ^{1}H-NMR spectroscopy for metabolite quantification. The sensitivity of the technique is in the low micromolar range for most metabolites. It is well suited to detect creatine in urine, plasma, and cerebrospinal fluid as well as *in-vivo* within the brain (overview and details taken from [2]). Here, ^{1}H-NMR spectra were acquired on an Achieva 3T MR scanner (Philips, Best, The Netherlands) using a PRESS sequence (TR=2000 ms, TE=35 ms, 128 averages, 15x15x15 mm voxel) and processed in LCModel (Provencher, Magn Reson Med 30, 672 (1993)), referencing to the unsuppressed water.

<u>Renal proximal tubular cell model</u>

A permanently transfected, inducible renal proximal tubular cell line derived from LLC-PK1 cells was created for each patient GATM mutation using recombinant technology. LLC-PK1 cells are an established model and reliably express many properties of the renal proximal tubule.[3] We previously had established tetracycline-inducible stable transfected LLC-PK1 cells that were obtained using the Flp-in T-Rex system (Invitrogen, Paisley, UK) containing the constructs pFRT/lacZeo and pcDNA/5/TR (JCRB0060, Health Science Research Resources Bank, Tokyo, Japan). These cell lines and derived cells were maintained in 1 g/L glucose DMEM (PAA laboratories, E15-005, Yeovil, UK) medium with 8% fetal bovine serum (PAA laboratories, A15-109, Yeovil, UK), 2 mM L-glutamine (PAA laboratories, M11-006, Yeovil, UK), penicillin (100 U/ml)/streptomycin (100 µg/ml) (PAA laboratories, P11-010, Yeovil, UK).

The human *GATM* coding region was obtained from a Trueclone full length cDNA clone (sc321307, NM_001482.1; Origene Technologies; Rockville, MD, USA). The Origene vector containing the full length *GATM* cDNA was subcloned into the *NotI* site of the pcDNA5FRT/TO vector. The patients' mutations c.958C>T (p.P320S), c.1006A>G (p.T336A), c.1007C>T (p.T336I), and c.1022C>T (p.P341L), were inserted via site-directed mutagenesis (QuikChange II, Stratagene, Santa Clara, CA USA). To this end the following oligo pairs were used:

5'-GTATTGTGCTTTCCAAC**T**CTGACCGACCATGTCAC-3',
5'-GTGACATGGTCGGTCAGAGTTGGAAAGCACAATAC-3' (c.958C>T);
5'-TCAAGAAAGCAGGATGG**G**CTATCATTACTCCTC-3',
5'-GAGGAGTAATGATAG**C**CCATCCTGCTTTCTTGA-3' (c.1006A>G);
5'-TCAAGAAAGCAGGATGGA**T**TATCATTACTCCTC-3',
5'-GAGGAGTAATGATA**A**TCCATCCTGCTTTCTTGA-3' (c.1007C>T);
5'-TCAAGAAAGCAGGAT̲GGA**T**TATCATTACTCCTCC-3',
5'-GGAGGAGTAATGATA**A**TCCATCCTGCTTTCTTGA-3' (c.1022C>T).

2

The full length wildtype and mutant cDNA clones were all sequence-verified. The stable transfected Frt-1 cells containing the pcDNA/5/TR construct were cotransfected at a ratio of 9:1 (w/w) circularized pOG44:pcDNA5/FRT/TO/GATM, pOG44:pcDNA5/FRT/TO/T336AGATM, pOG44:pcDNA5/FRT/TO/T336IGATM, pOG44:pcDNA5/FRT/TO/P341LGATM, or pOG44:pcDNA5/FRT/TO/P320SGATM. Transfection was performed using lipofectamine 2000 (Thermofisher Scientific, 11668027, UK) according to the protocol of the manufacturer. The transfected cells were incubated for four weeks in selection medium containing 500 μg/ml hygromycin-B. Several clones were obtained for cells transfected with these constructs. Incorporation of the constructs in the genomic DNA was demonstrated by PCR analysis, and subsequently sequence analysis of the full coding region of human *GATM*. These PCR and sequence conditions are available on request. Induced expression of human *GATM* was achieved using 1 μg/ml tetracycline (Applichem/VWR, A1685, Lutterworth, UK) for each of the clones. To this end, real-time PCR (conditions used available on request), Western analysis (conditions used available on request) and immunohistochemical analysis were utilized. For all functional analyses described, a single clone was used. Upon induction with 1 μg/ml tetracycline these clones showed equal expression of human *GATM*.

RNA isolation

Inducible LLC-PK1 cells were seeded in cell medium (RPMI medium 1640 with 11.1 mM glucose (Gibco Cell Culture Systems - Invitrogen, Karlsruhe, Germany), FCS 10%, penicillin G 5 I.U., streptomycin 50 μg/ml, sodium hexanoate 5 mM). To induce the expression system of the cells, tetracycline (1 μg/ml) was added to the medium. Cells were cultured and induced for three weeks until RNA was isolated. Medium was changed every other day. Total RNA from inducible LLC-PK1 cells was isolated using a column based kit optimized for the purification from small amounts of tissue according to the manual (RNeasy Micro Kit, Qiagen, Hilden, Germany). The RNA concentration was quantified with a photometer (NanoDrop ND-1000, PEQLAB Biotechnologie GmbH, Erlangen, Germany). Quality of the RNA used for real-time RT-PCR was tested by agarose electrophoresis.

Quantitative realtime PCR

Reverse transcription with M-MLV-RT (Promega GmbH, Mannheim, Germany) and random primers (Fermentas GmbH, St. Leon-Rot, Germany) was done using 1 μg total RNA to generate single-stranded cDNA. Relevant contamination with genomic DNA was excluded by negative control reactions without the reverse transcriptase enzyme (-RT). Realtime PCR of cDNA samples was performed on a LightCycler 480 device (Roche, Basel, Switzerland) using specific and, wherever applicable, intron-spanning primers, and a SYBR® Green mastermix (Roche, Basel, Switzerland). Target gene expression levels were quantified relative to beta-actin expression under consideration of PCR efficiencies calculated on the basis of standard dilution curves. The specificity of PCR amplifications was verified by agarose electrophoresis and melting curve analysis. Primer sequences (Life Technologies GmbH, Darmstadt, Germany) are listed in Table S3.

For realtime-PCR experiments in LLC-PK1 cells (porcine NLRP3, porcine IL-18, porcine FN1, porcine ACTA2, Fig. 3J, K and Fig. 4A, B), n=20 petri dishes of three independent experimental series were used (each series with vector control cells and cells over-expressing wildtype GATM or the T336A mutant). For realtime PCR experiments determining the murine GATM expression in mouse kidneys after a high creatine diet, n=4 treated and n=4 untreated animals were used. Data are shown as

3

1
2
3
4
5
6
7
8
9
10
11
12
13
14
15
16
17
18
19
20
21
22
23
24
25
26
27
28
29
30
31
32
33
34
35
36
37
38
39
40
41
42
43
44
45
46
47
48
49
50
51
52
53
54
55
56
57
58
59
60

mean values ± standard error of the mean (SEM); "n" stands for the number of observations. ANOVA followed by a Bonferroni Test (OriginPro, Northampton, MA 01060, USA) (Fig. 3J, K and Fig. 4A, B) or *t*-test (Fig. 4E) were used to determine statistical significance. A p-value of 0.05 was accepted to indicate statistical significance.

Immunofluorescence on inducible LLC-PK1 cells

Inducible LLC-PK1 cells were grown on glass coverslips and induced with tetracycline (1 µg/ml) for at least 24 h. For mitochondrial staining, MitoTracker Orange CMTMRos (Invitrogen, Karlsruhe, Germany) was added (1:5000) to the medium and incubated at 37℃, 5% CO_2, for 30 min. After washing with Ringer's solution, cells were fixated for 15 min with 3% paraformaldehyde in PBS (phosphate buffered saline pH 7.4). Cells were rinsed twice with PBS and afterwards incubated in PBS containing 0.1% SDS for 5 min to unmask the epitopes followed by another wash with PBS for 2 x 5 min. Primary antibodies were applied for 1 h. Primary and secondary antibodies were diluted in PBS with 0.04% Triton X-100 (Sigma, Taufkirchen, Germany). After washing twice (PBS, 5 min), cells were incubated for 1 h with the secondary antibody and HOE33342 to stain the nuclei. After a final washing step (PBS, 2 x 5 min), the glass coverslips with the cells were mounted on slides with fluorescent-free glycergel mounting medium (DakoCytomation, Hamburg, Germany). A list of all used primary and secondary antibodies as well as further dyes is provided in Table S3.

Analysis of plasma and urine of Gatm$^{+/+}$ and Gatm$^{-/-}$ mice

Spot urine of 9 - 12 week old Gatm$^{+/+}$ (n=6) and Gatm$^{-/-}$ (n=6) mice was collected twice per mouse on two different days. After the last sample was taken, mice were sacrificed and blood was collected. Metabolites of the creatine synthesis pathway (creatinine, creatine, guanidinoacetate), blood glucose, and amino acids were measured in urine and plasma. All urine values were normalized to urinary osmolality. For measurements urine samples were diluted 1:4. Amino acids were derivatized with propylchloroformate/propanol and measured by LC-MS/MS with electrospray ionization in positive mode and detection by multiple reaction monitoring (MRM) as recently described.[4] 5 µl of diluted urine or plasma were used for derivatization. Quantification was based on calibration curves using ^{13}C,^{15}N-labeled amino acids as internal standards.

Creatinine, creatine, and guanidinoacetate were analyzed by LC-MS/MS with electrospray ionization (ESI) in positive mode. An Agilent 1200 SL HPLC hyphenated to an AB Sciex (Darmstadt, Germany) 4000 QTrap mass spectrometer working with a TurboV electrospray ion source was used. HPLC separation was performed on an Atlantis T3 reversed-phase column (150 mm × 2.1 mm i.d., 3 µm, Waters, Eschborn, Germany) with mobile phases A (0.1% formic acid in water, v/v) and B (0.1% formic acid in acetonitrile, v/v) employing a flow rate of 350 µl/min. The following gradient was used with deviating parameters for the positive mode ionization run given in brackets: 0–10 min linear increase from 0% to 100% B, hold for 2 min (0 min) and return to 0% B at 12.1 min (10.1 min) and equilibrate for 7 min. The column was kept at 25℃. An injection volume of 10 µl was used. Analytes were detected in MRM mode. For the analysis in positive mode ionization, two time segments were programmed detecting different analytes. Quantification was based on calibration curves using the stable isotope-labelled analogues as internal standards. Creatinine-d3 was used as internal standard for creatine and guanidinoacetate, because they eluted close to each other.

10 µl internal standard (IS1) solution, containing creatinine-d3 at a concentration of 100 µM, were added to 10 µl pre-diluted urine and further diluted with water to a final volume of 100 µl. A plasma aliquot of 25 µl was spiked with 5 µl IS1 solution and 10 µl

4

surrogate solution containing [U-^{13}C]glucose, [U-^{13}C]lactic acid, and [U-^{13}C]pyruvic acid at a concentration of 1 mM. Proteins were precipitated with 150 µl cold methanol and samples were centrifuged for 5 min at 4°C and 11200 g. The supernatant was collected and dried using a vacuum evaporator (CombiDancer, Hettich AG, Bäch, Switzerland). The residue was redissolved in 100 µl water and subjected to analysis.

p-values for urine analysis: Creatinine = 0.0002, Creatine = 0.0140, Guanidinoacetate = 0.0001. p-values for plasma analysis: Creatinine = 0.0026, Creatine = 0.0010, Lactate = 0.0031, Serine = 0.0021, Threonine = 0.0017. Data are shown in mean values ± standard error of the mean (SEM); "n" stands for the number of observations. An unpaired *t*-test was used to determine statistical significance. As multiple parameters were tested in urine and plasma, p-values were corrected according to Bonferroni correction (0.05/ n). p-values of 0.0167 (metabolites of the creatine pathway), 0.0167 (metabolites of the energy pathway), and 0.0025 (amino acids) were accepted to indicate statistical significance.

Immunofluorescence on cryo sections

Cryosections (5 µm) were mounted on poly-L-lysine slides (Kindler, Freiburg, Germany). Prior to incubation with the primary antibodies, sections were incubated in 0.1% SDS (5 min) for unmasking of epitopes, washed in PBS (2 x 5 min) followed by blocking with 5% bovine albumin (10 min). Primary and secondary antibodies were diluted in phosphate buffered saline (PBS), pH 7.4, with 0.04% Triton X-100 (Sigma, Taufkirchen, Germany). Primary antibodies were applied overnight at 4°C. After washing with PBS (2 x 5 min), sections were incubated for 1 h with the secondary antibodies and HOE33342 to stain the nuclei. The slides were then washed in PBS (2 x 5 min) and mounted with fluorescent-free glycergel mounting medium (DakoCytomation, Hamburg, Germany). A list of all used primary and secondary antibodies as well as further dyes is provided in Table S3.

Immunofluorescence on paraffin sections

Human kidney samples were embedded in paraffin and slices (5 µm) were mounted on poly-L-lysine slides (Kindler, Freiburg, Germany). To remove paraffin from the tissues, slides were put into xylol twice for 10 min each and afterwards rehydrated in an alcohol series (99% isopropanol, 95% EtOH, 80% EtOH, 70% EtOH) for 10 min each. Then, slices were rinsed with PBS for 5 min and heated at 95°C in citrate buffer (pH 6.0) for 15 min to unmask epitopes. The rest of the protocol was performed according to the protocol for cryosections. A list of all used primary and secondary antibodies as well as further dyes is provided in Table S3.

Masson-Goldner staining on paraffin sections

For Masson-Goldner staining, sections were deparaffinized as described above. Afterwards, slices were incubated in Weigert's Iron Hematoxylin solution for 2 min, rinsed in running tap water for 2 min and then briefly put into 0.1% HCl-alcohol solution. Subsequently, the slices were rinsed in running tap water for 10 min, incubated in 0.5% phosphor tungistic acid for 15 sec and washed three times for 5 min each in distilled water, before they were stained in fuchsine acid and Ponceau for 10 min. Next, slides were incubated 3 times each for 1 min in 1% glacial ethanoic acid, 20 sec in orange G-solution, 2 min in 1% glacial ethanoic acid, 4 min in lightgreen-solution and rinsed twice in 2% glacial ethanoic acid. Afterwards, slices were dehydrated in 96% isopropanol (20 sec), 99% isopropanol (twice for 5 min each) and xylol (twice for 10 min each). The slides were mounted with xylol-containing DEPEX-medium.

Electron microscopy and immunogold labeling

Kidney specimens of our Fanconi patients were originally embedded in paraffin. For electron microscopy, samples were deparaffinized according to the following protocol: xylol (2 x 15 min, 3 x 30 min), 100% ethanol (5 x 15 min), 95% ethanol (15 min), 90% ethanol (15 min), 70% ethanol (15 min), 50 % ethanol (15 min), distilled water (2 x 15 min). After post fixation with 4% glutaraldehyde solution (in 0.1 M Na-cacodylate pH 7.4 for 60 min) samples were finally rinsed with 0.1 M Na-cacodylate pH 7.4 (2 x 15 min).

Inducible LLC-PK1 cells were grown on cover slips and induced with tetracycline (1 µg/ml) for 3 d. Before embedding, cells were fixed using a 2% glutaraldehyde solution in 0.1 M Na-cacodylate pH 7.4 for about 1 h. Post fixation and dehydration of the samples was carried out using the following protocol: rinsing in 0.1 M Na-cacodylate pH 7.4 (3 x 20 min), 1% OsO4 in 0.1 M Na-cacodylate pH 7.4 (2 h), 0.1 M Na-cacodylate pH 7.4 cacodylic acid (3 x 20 min), 50% ethanol (15 min), 70% ethanol (15 min), 90% ethanol (15 min), 96% ethanol (15 min), 100% ethanol (20 min), acetone (3 x 15 min). Finally, samples were embedded in Epon and polymerized at 60°C for 48 h using standard protocols. For immunogold labelling, freshly prepared ultrathin sections (70 nm; Ultracut UC6; Leica, Wetzlar, Germany) were mounted on grids and treated according to the following protocol: 0.1% glycine in PBS (5 min), 1% BSA in glycine solution (5 min), primary antibody against GATM in 0.1% BSA in PBS for 1.5 h, 0.1% BSA in PBS (5 x 2 min), secondary antibody (goat anti rabbit 6 nm gold particles; Aurion, Wageningen, Netherlands) in 0.1% BSA in PBS for 1.5 h, 0.1% BSA in PBS (5 x 2 min), PBS (2 x 2 min), 2% glutaraldehyde in PBS (5 min), PBS (2 x 2 min), distilled water (3 x 2 min). To improve contrast, specimens were stained with 2% UAc for 30 min. Ultrathin sections were imaged using either an EM902 (Zeiss, Oberkochen, Germany) or a JEM-2100F (JEOL, Tokyo, Japan) transmission electron microscope, operated at 80keV (902) or 200 keV (JEM). Digital micrographs were recorded using a CCD 2k camera (Troendle, Moorenweis, Germany) or a CMOS 4k F416 camera (TVIPS, Gauting, Germany).

Quantification of intracellular IL-18 in inducible LLC-PK1 cells

Quantification of intracellular IL-18 protein content in induced LLC-PK1 cells was performed using an ELISA Kit form PromoKine (PK-EL-62816P, Heidelberg, Germany) recognizing porcine IL-18. The ELISA was performed according to the manufacturer's protocol. n =3 petri dishes were used for LLC-PK1 cells over-expressing the wildtype protein or the T336A mutant, respectively. Cells were induced with tetracycline for 2 weeks. In the following week, tetracycline was removed from the medium. After 3 weeks, cells were lysed and intracellular content of IL-18 was quantified. Data were normalized to total protein content determined by Bradford assay. p-value = 0.0012. Data are shown as mean values ± standard error of the mean (SEM); "n" stands for the number of observations. An unpaired *t*-test was used to determine statistical significance and a p-value of 0.05 was accepted to indicate statistical significance.

Determination of protein concentration with Bradford assay

Frozen cell pellets were used to determine protein concentration of inducible LLC-PK1 cells. Cell pellets were resuspended in sample buffer containing DTT, 86% glycerol, 10 % SDS, 0.5 M tris(hydroxymethyl)aminomethane (TRIS) pH 6.8, 0.5 M $MgCl_2$, and 25 U/µl benzonase. For quantification, different BSA solutions of known concentration were prepared. All samples were diluted in Bradford reagent (1:100) and transferred to a 96-well plate. After incubating for 15 min in the dark, the absorption at 595 nm was measured in a microplate reader (Bio-Rad, Hercules, USA). Protein concentrations were determined on the basis of the standard linear slope from the BSA standards.

6

Measurement of extracellular LDH activity

For over-expression of wildtype GATM or T336A mutant proteins, respective LLC-PK1 cells were induced with tetracycline for 3 weeks (plus the days shown on the x-axis in the graph of Fig. 4C). Extracellular LDH activity as a surrogate marker of cytolysis was measured using Pierce™ LDH cytotoxicity assay kit (Thermo Fisher Scientific, Bonn, Germany). The experiments were carried out in triplicate and normalized to the total cellular protein amounts determined by Bradford assay. Significant differences were determined in IBM SPSS 23 using two-way ANOVA with post-hoc Student´s t-tests corrected for multiple testing by the Bonferroni method ($0.05/n = 0.0167$). p-values were 0.0039 (day 2), <0.0001 (day 3), and <0.0001 (day 4). Data are shown as mean values ± standard error of the mean (SEM); "n" stands for the number of observations.

Live cell imaging of mitochondrial reactive oxygen species production

3.5×10^5 LLC-PK1 cells were seeded on a 30-mm cover glass coated with poly-L-lysine. When confluent, cells were incubated with 1 µg/ml tetracycline for 48 h to induce expression of wildtype- or mutant T336A GATM. Reactive oxygen species (ROS) production was measured by incubating the cells with 5 µM CellROX Deep Red (Life Technologies) for 30 min at 37°C. The rate of increase in fluorescence signal was taken as proportional to the rate of ROS production. Cells were imaged at 37°C using a Leica SP5 automated inverted confocal laser scanning microscope and a 63x objective. CellROX was excited at 633 nm and light was collected between 638 nm and 737 nm. Images were acquired every 10 min to minimize laser-induced photo-toxicity for a maximal duration of 40 min. 7 coverslips of induced wildtype and 6 of mutant T336A GATM were imaged. 30 fields were acquired per coverslip using the Matrix screener Leica software and normalized to the initial fluorescence after incubation (30 min with CellROX). Images were analyzed using Image J software (https://imagej.nih.gov/ij/). The results are presented as mean values ± SEM. Statistical analysis was performed using Prism 6 (http://www.graphpad.com) by comparing the rates of ROS production between wildtype and mutant cells using a linear regression analysis (equivalent to analysis of covariance (ANCOVA)).

Creatine supplementation

Male, wildtype C57Bl/6 mice (n=8, age 10 weeks, Jackson Laboratories) were randomly assigned to either a group nourished with a diet consisting of bread and tap water (low creatine, high carbohydrate diet) or a group with an additional supplement of 1% (w/w) creatine (Sigma-Aldrich Chemie GmbH, Steinheim, Germany) in the drinking water. After sacrificing the mice kidneys were removed, divided into halves, then immediately frozen in liquid nitrogen and stored at -80°C until further experimentation. Frozen mouse kidneys were pulverized in liquid nitrogen using a mortar and RNA was isolated using RNeasy Mini Kit (Qiagen GmbH, Hilden, Germany) according to the manufacturer's recommendations. RNA was quantified using the NanoDrop 2000c spectrophotometer (Peqlab Biotechnologie GmbH, Erlangen, Germany) and its quality was assessed by imaging on 1% agarose gel. RNA was then transcribed to cDNA using Reverse Transcription System (Promega, Madison, WI) according to the manufacturer's recommendations. Real-time PCR was performed as described above using cDNA, SYBR® Green mix (Roche Diagnostics GmbH, Mannheim, Germany) and primers for mouse Gatm or β-actin (Table S4). For real-time PCR, a Light Cycler 480 (Roche Diagnostics, Rotkreuz, Switzerland) was employed according to the manufacturer's recommendations. Quality and size of the amplicon were further verified by visualization on 3% agarose gels.

7

Frozen mouse kidneys were weighed, then pulverized in liquid nitrogen using a mortar and proteins eluted by incubation in 3 µl/mg kidney tissue of a lysis-buffer containing RIPA-buffer (1% Igepal CA-630, 0.5% sodium-desoxycholate, 0.1% SDS in PBS), 200 mM PMSF (1/200 v/v) and EDTA-free protease inhibitor cocktail set III (1/100 v/v, Calbiochem, San Diego, CA) for 20 min on ice. Samples were centrifuged at 14.800 rpm for 10 min at 4℃ and supernatants stored at -20℃ until further analysis. The protein content of the samples was quantified in 96-well plates (Nuncleon Delta Surface, NUNC A/S, Roskilde, Denmark) according to Bradford using Bio-Rad protein assay (Bio-Rad Laboratories GmbH, Muenchen, Germany) and Bio-Rad 550 Microplate Reader (Bio-Rad) according to the manufacturer's recommendations. Equal amounts of proteins in Laemmli-buffer (Bio-Rad) including 2-mercaptoethanol 1/20 (v/v, Merck Schuchard, Hohenbrunn, Germany) were cooked for 5 min, separated by 10% SDS-PAGE and transferred to a PVDF blotting membrane (Amersham Hybond). The membrane was blocked by incubation with 5% fat-free dry milk-powder (w/v, AppliChem GmbH, Darmstadt, Germany) in PBS-Tween for 1 h at room temperature followed by incubation with primary antibody polyclonal rabbit anti-GATM (1/2000 v/v, Proteintech, Manchester, UK) in 1.5% BSA in PBS-Tween at 4°C overnight. The secondary antibody donkey anti-rabbit IgG-horseradish peroxidase (HRP, 1/5000, v/v, Santo Cruz Biotechnology) in 1% PBS-Tween was incubated for 1 h at room temperature and protein bands developed using Western Blot Luminol Reagent (Santa Cruz Biotechnology, Heidelberg, Germany) and visualized in Fusion Fx7 (Vilber Lourmat, Marne-la-Vallee, France). The membranes were stripped from bound antibodies by applying Restore Western Blot Stripping Buffer (Thermo Scientific, Rockford, IL) for 15 min at room temperature, washed, blocked as described above and the house-keeping protein was detected using as primary antibody rabbit anti-mouse beta-actin (1/5000 v/v, Sigma-Aldrich, Taufkirchen, Germany) in 1.5% BSA-PBS-Tween at 4℃ overnight and as secondary antibody donkey anti-rabbit IgG-HRP (1/5000, v/v, Santa Cruz Biotechnology, Heidelberg, Germany) in 1% PBS-Tween for 1 h at room temperature. Quantification of Gatm and beta-actin was performed with ImageJ.

p-values: RT-PCR = 0.0125, Western blot quantification = 0.029 . Data are shown in mean values ± standard error of the mean (SEM); "n" stands for the number of observations. An unpaired *t*-test was used to determine statistical significance and a p-value of 0.05 was accepted to indicate statistical significance.

Structural studies and data availability

To test the hypothesis of mutation-mediated aggregation of GATM, we performed molecular dynamics simulations on the wildtype monomer and on the four mutants. Modelling of possible protein-protein interaction surfaces (GRAMM-X; http://vakser.bioinformatics.ku.edu/resources/gramm/grammx/) started with the structure of the wildtype monomer (pdb: 1JDW at http://www.rcsb.org/pdb/home/home.do).

We utilized publicly available GATM crystal structures (i.e. 1JDW subunit A) to simulate the effect of all mutations recognized in our patients. In order to test the hypothesis of mutation-mediated destabilization of the region around B4, we performed molecular dynamics simulations on the wildtype monomer and on the four mutants, starting from the coordinates of 1JDW subunit A. Each simulation lasted for 40 ns. At the end of the simulations (after 40 ns) superposing all the mutants on the wildtype protein results in Cα root mean square displacement (r.m.s.d.) from 1.12 to 1.47 Å (from 1.17 to 1.72 Å if we limit the superposition on the region around the B4 surface). The lower differences with respect to the wildtype in T336A mutant could be related to the fact that this mutation may require more time (with respect to the 40 ns of the simulation) to propagate its effect.

In order to test the possibility of stable dimerization based on the B4 surface, we performed two additional molecular dynamics simulations on the wildtype and on the P341L B4-based dimers as modelled by the program GRAMM-X. The P341L mutant was chosen being the one with the higher overall r.m.s.d. respect to wildtype GATM during the previous simulations, therefore the most variable during the simulation time.

Along the simulation, the wildtype dimer analyzed by the program PISA (www.ebi.ac.uk/pdbe/pisa/) adopts different configurations compatible with stable and unstable dimeric assemblies. Interestingly, the P341L dimer promptly evolves toward stability (after 10 ns) that is maintained along the remaining simulation time. Such simulation results show, on one hand, how the B4 interface is prone to protein-protein interaction also in the wildtype protein and, on the other hand, how it is sufficient for only a point mutation (P341L) to shift the B4 based monomer-dimer equilibrium towards another stable quaternary assembly. This analysis, as the one shown before, clearly supports the hypothesis that the mutation induced structural rearrangements of the B4 surface do promote a new protein-protein interaction surface that can lead to linear aggregation of GATM.

For cell expression studies, the human GATM coding region obtained from a Trueclone full length cDNA clone (sc321307, https://www.ncbi.nlm.nih.gov/nuccore/NM_001482.1; Origene Technologies; Rockville, MD, USA) was used.

9

1
2
3
4
5
6
7
8
9
10
11
12
13
14
15
16
17
18
19
20
21
22
23
24
25
26
27
28
29
30
31
32
33
34
35
36
37
38
39
40
41
42
43
44
45
46
47
48
49
50
51
52
53
54
55
56
57
58
59
60

Supplementary Figures

<u>Figure S1</u>
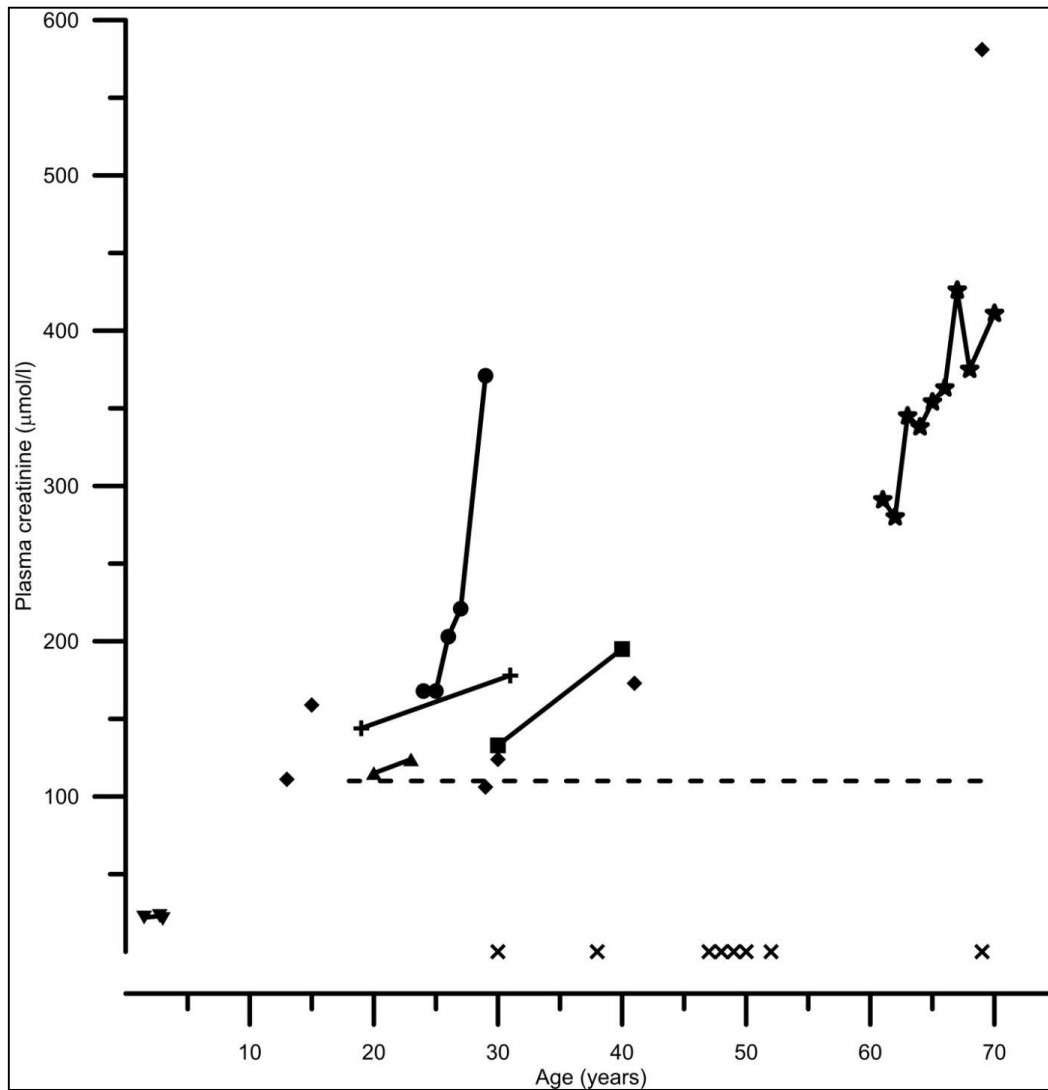
Graph illustrating decline in kidney function in GATM related renal Fanconi syndrome and kidney failure and age at kidney transplantation. Data from affected and genotyped individuals are shown. In six individuals (▼, +, ▲, ●, ■, ✱) connecting lines indicate serial measurements. In another six individuals (♦) single creatinine measurements are plotted. In eight individuals (✗) age at kidney transplantation is presented. The horizontal dashed line indicates normal plasma creatinine (110 µmol/l) for an average adult person. Note normal plasma creatinine in the youngest child and ensuing kidney failure in individuals from adolescence on with need for transplant as early as 30 years of age.

10

Figure S2
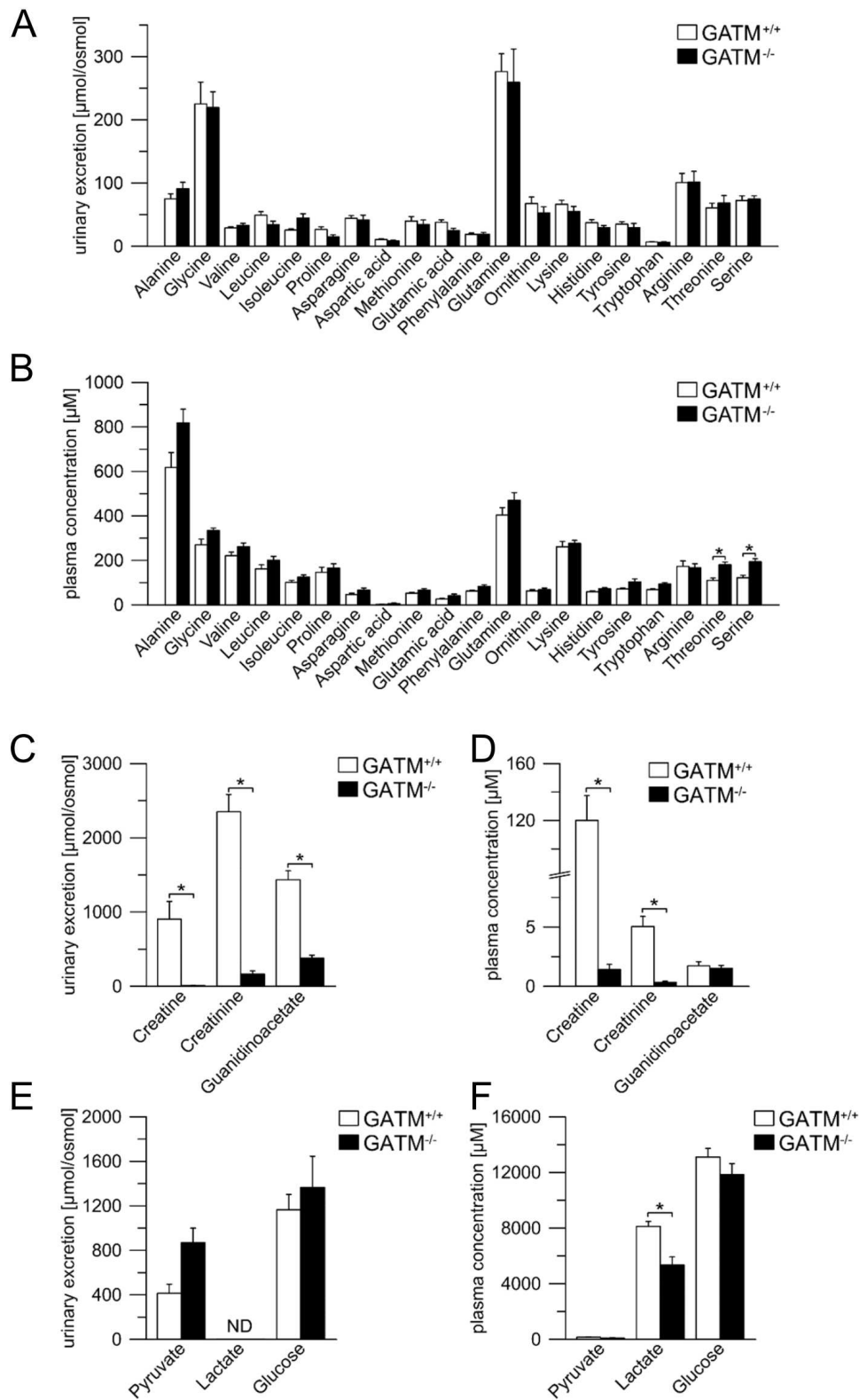
Analysis of urine and plasma from *Gatm+/+* and *Gatm**-/-* mice: (A)** Urinary excretion of amino acids as well as glucose excretion was not different between *Gatm**+/+* and *Gatm**-/-* mice (n=6/6, values normalized to osmolyte excretion), which indicates that knockout animals do not suffer from renal Fanconi syndrome. **(B)** In plasma, the concentrations of most amino acids and glucose (non-fasted animals) were similar between the two groups. **(C and D)** As expected, urine and plasma concentrations of creatine and creatinine were very low in *Gatm**-/-* mice, since the endogenous creatine synthesis pathway is disturbed. The residual creatine and creatinine amounts result from creatine absorption from food. Interestingly, the concentration of guanidinoacetate, the direct product of Gatm activity, was normal in plasma whereas the urinary excretion was decreased in knockout mice. **(E)** Urinary excretion of pyruvate, lactate and glucose. **(F)** Plasma concentration of lactate was lower in *Gatm**-/-* mice whereas pyruvate concentration was not different. ND = not detectable.

Parameters for LC-MS/MS analysis used in Fig. S2:

Analyte	Ionization mode	Q1 (m/z)	Q3 (m/z)	Dwell time (ms)	DP
Creatinine	positive –P1	114.0	86.0	150	26
Creatinine d3	positive –P1	117.0	89.0	150	26
Creatine	positive –P1	132.2	90.0	150	21
Guanidinoacetate	positive –P1	118.1	43.0	150	36

DP - declustering potential, P1 - period 1, P2 - period 2

12

Figure S3
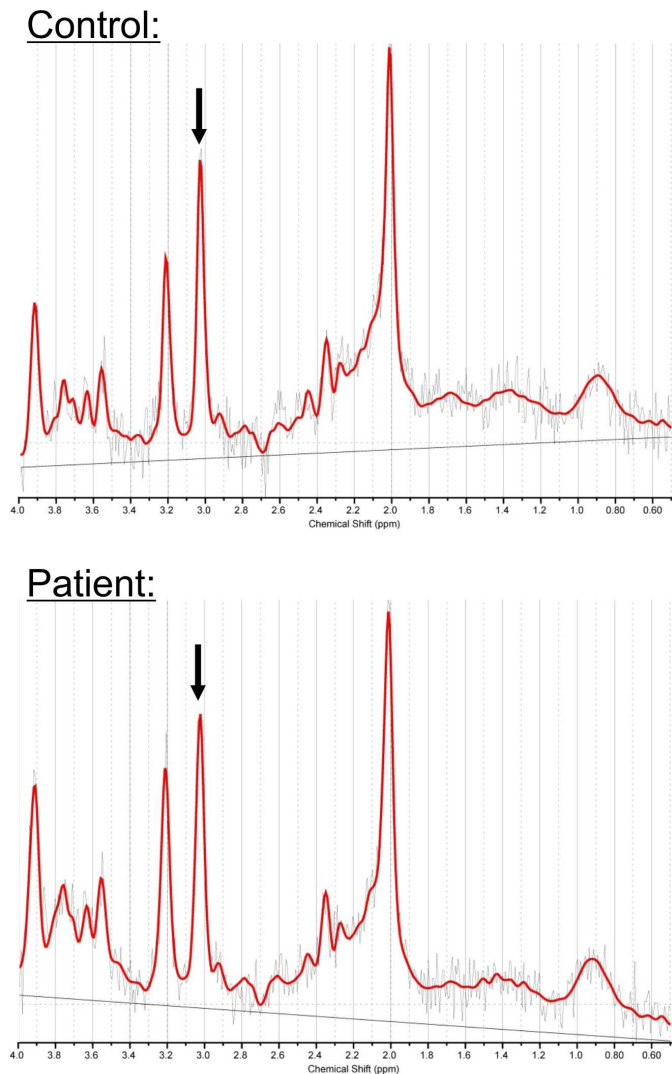
Control:

Patient:

[1]**H-NMR spectroscopy to determine brain (grey matter) creatine content:** Note, normal creatine (total) peak (indicated by arrow) in control volunteer (top) and GATM patient (bottom), providing also evidence for GATM's catalytical (i.e. enzymatic) competence. Quantification in the volunteer showed a total creatine of 5.8 mM and 5.0 mM in grey and white matter, respectively. The GATM patient showed 6.1 mM and 4.4 mM in grey and white matter, respectively.

13

Supplemental Tables

<u>Table S1</u>
Laboratory findings of a young patient with GATM-related renal Fanconi syndrome

Substance	Laboratory finding	Age appropriate reference ranges
Plasma values		
Sodium	143 mmol/L	133 - 146 mmol/L
Potassium	3.6 mmol/L	3.5 - 5.5 mmol/L
Chloride	108 mmol/L	100 - 108 mmol/L
Total CO_2	17 mmol/L	20 - 30 mmol/L
Urea	5.3 mmol/L	2.5 - 6.0 mmol/L
Creatinine	22 µmol/L	16 - 33 µmol/L
Calcium	2.47 mmol/L	2.17 - 2.44 mmol/L
Magnesium	0.95 mmol/L	0.66 - 1.00 mmol/L
Phosphate	1.16 mmol/L	1.2 - 2.1 mmol/L
Albumin	49 g/L	34 - 42 g/L
Alkaline Phosphatase (ALP)	413 U/L	145 - 320 U/L
Alanine Transaminase (ALT)	30 U/L	5 - 45 U/L
Total bilirubin	5 µmol/L	< 18 µmol/L
Intact PTH	2.5 pmol/L	0.7 - 5.6 pmol/L
Urine values		
Glucose Stix result	positive +++	negative
Glucose	8.0 mmol/L	
Phosphate	8.86 mmol/L	
Creatinine	0.5 mmol/L	
Phosphate/Creatinine ratio	17.72	1.2 - 14
Tubular Reabsorption of Phosphate	66 %	70 - 100 %
TmP/GFR	0.77 mmol/L	1.10 - 2.70 mmol/L
Urine amino acids		
Glycine/Creatinine ratio	5090 µmol/mmol	250 - 626 µmol/mmol
Serine/Creatinine ratio	2355 µmol/mmol	20 - 100 µmol/mmol
Threonine/Creatinine ratio	2129 µmol/mmol	10 - 45 µmol/mmol
Proline/Creatinine ratio	1864 µmol/mmol	0 - 3 µmol/mmol
Leucine/Creatinine ratio	320 µmol/mmol	3 - 10 µmol/mmol
Isoleucine/Creatinine ratio	141 µmol/mmol	2 - 10 µmol/mmol
Valine/Creatinine ratio	738 µmol/mmol	2 - 8 µmol/mmol
Alanine/Creatinine ratio	3092 µmol/mmol	30 - 80 µmol/mmol
Glutamine/Creatinine ratio	4159 µmol/mmol	30 - 120 µmol/mmol
Arginine/Creatinine ratio	166 µmol/mmol	2 - 10 µmol/mmol
Ornithine/Creatinine ratio	230 µmol/mmol	2 - 10 µmol/mmol
Lysine/Creatinine ratio	1614 µmol/mmol	5 - 30 µmol/mmol
Cystine/Creatinine ratio	226 µmol/mmol	5 - 25 µmol/mmol
Methionine/Creatinine ratio	46 µmol/mmol	3 - 15 µmol/mmol
Taurine/Creatinine ratio	184 µmol/mmol	30 - 105 µmol/mmol
Phenylalanine/Creat ratio	345 µmol/mmol	5 - 15 µmol/mmol
Tyrosine/Creatinine ratio	716 µmol/mmol	5 - 15 µmol/mmol
Tryptophan/Creatinine ratio	193 µmol/mmol	1 - 5 µmol/mmol
Histidine/Creatinine ratio	1909 µmol/mmol	100 - 300 µmol/mmol
Aspartate/Creatinine ratio	82 µmol/mmol	10 - 35 µmol/mmol

14

Glutamate/Creatinine ratio	86 µmol/mmol	0 - 3 µmol/mmol
Albumin/Creatinine ratio	54.3 mg/mmol	1.5 - 8.7 mg/mmol
NAG/Creatinine ratio	392 U/mmol	2 - 22 U/mmol
Retinol Binding Protein/Creatinine ratio	10420 µg/mmol	2.7 - 103 µg/mmol

Laboratory findings from an affected and genotyped 18 month old child before start of treatment illustrating presence of renal Fanconi syndrome. Note normal plasma creatinine and normal PTH. Note typical signs of renal Fanconi syndrome, i.e. glucosuria, hyperphosphaturia and hypophosphatemia, generalized hyperaminoaciduria, low molecular weight proteinuria, metabolic acidosis and slightly elevated alkaline phosphatase (in red).

Table S2

PCR primer sequences and PCR conditions for expression studies

Gene	Acc. no.	Primer	Sequence (5'>3')	Annealing temp.
murine *GATM*	NM_025961.5	sense	TTTTCAAGAAAGCAGGATGGA	57°C
		antisense	TGACATCCAGAGGGGATGAT	
porcine *FN1*	XM_003133643.2	sense	GAGGCACAAGATTCGGGAGG	61°C
		antisense	CATAATGGGAAACCGTGTAGGG	
porcine *ACTA2*	NM_001164650.1	sense	AGAACACGGCATCATCACCA	61°C
		antisense	CAGGGTCGGATGCTCTTCTG	
porcine *IL-18*	NM_213997	sense	AGCTGAAAACGATGAAGACCTG	61°C
		antisense	AAACACGGCTTGATGTCCCT	
porcine *NLRP3*	NM_001256770	sense	CCTGCAAAAACTGGGGTTGG	60°C
		antisense	CTCCAAGAGCATTTCCCCGT	
porcine *β-actin*	ENSSSCT00000008324	sense	CCCATCTACGAGGGGTACG	60°C
		antisense	CGCTCCGTCAGGATCTTC	
murine *β-actin*	NC_000085.6	sense	GACAGGATGCAGAAGGAGATTACTG	57°C
		antisense	CCACCGATCCACACAGAGTACTT	

Table S3

Antibodies and conditions for imaging studies. IF: immunofluorescence, WB: Western blot.

Antibody/Dye (Usage)	Species	Dilution	Manufacturer
anti-GATM (IF, WB)	rabbit	1:200 (IF) 1:2000 (WB)	Proteintech, Manchester, UK
anti-α-SMA (IF)	mouse	1:600	Abcam, Cambridge, UK
anti-β-actin (WB)	rabbit	1:5000	Sigma-Aldrich, Taufkirchen, Germany
Alexa Fluor® 555 anti rabbit (IF)	donkey	1:400	Invitrogen, Karlsruhe, Germany
Alexa Fluor® 488 anti mouse (IF)	donkey	1:400	Invitrogen, Karlsruhe,

15

			Germany
anti rabbit IgG-HRP (WB)	donkey	1:5000	Santa Cruz, Heidelberg, Germany
MitoTracker Orange CMTMRos (IF) (Stock: 1 mM)		1:5000	Invitrogen, Karlsruhe, Germany
HOE33342 (IF) (Stock: 5×10^{-4} M)		1:1000	Invitrogen, Karlsruhe, Germany

References

1. Joncquel-Chevalier, CM, Voicu, PM, Fontaine, M, Dessein, AF, Porchet, N, Mention-Mulliez, K, et al.: Creatine biosynthesis and transport in health and disease. *Biochimie,* 119**:** 146-165, 2015.
2. Engelke, U, Moolenaar, S, Hoenderop, S, Morava, E, van der Graaf, M, Heerschap, A, et al.: *Handbook of 1H-NMR spectroscopy in inborn errors of metabolism: body fluid NMR spectroscopy and in vivo MR spectroscopy,* Heilbronn, SPS Verlagsgesellschaft, 2007.
3. Klootwijk, ED, Reichold, M, Helip-Wooley, A, Tolaymat, A, Broeker, C, Robinette, SL, et al.: Mistargeting of peroxisomal EHHADH and inherited renal Fanconi's syndrome. *N Engl J Med,* 370**:** 129-138, 2014.
4. van der Goot, AT, Zhu, W, Vazquez-Manrique, RP, Seinstra, RI, Dettmer, K, Michels, H, et al.: Delaying aging and the aging-associated decline in protein homeostasis by inhibition of tryptophan degradation. *Proc Natl Acad Sci U S A,* 109**:** 14912-14917, 2012.

16